*Review Article*

# Molecular and Supramolecular Chirality: R2PI Spectroscopy as a Tool for the Gas-Phase Recognition of Chiral Systems of Biological Interest

MAURIZIO SPERANZA,[1] FLAMINIA RONDINO,[1] MAURO SATTA,[2] ALESSANDRA PALADINI,[3]
ANNA GIARDINI,[3] DANIELE CATONE,[4] AND SUSANNA PICCIRILLO[5]*

[1]*Dipartimento di Studi di Chimica e Tecnologia delle Sostanze Biologicamente Attive,
Università di Roma "La Sapienza", Roma, Italy*
[2]*CNR- ISC (Istituto dei Sistemi Complessi), Roma, Italy*
[3]*CNR-IMIP (sezione Istituto Materiali Speciali), Tito Scalo (Pz), Italy*
[4]*CNR-ISM (Istituto di Struttura della Materia), Roma, Italy*
[5]*Dipartimento di Scienze e Tecnologie Chimiche, Università di Roma "Tor Vergata", Rome, Italy*

*Dedicated to Professor Domenico Misiti on the occasion of his 75th birthday.*

*ABSTRACT* In life sciences, diastereomeric chiral molecule/chiral receptor complexes are held together by a different combination of intermolecular forces and are therefore endowed with different stability and reactivity. Determination of these forces, which are normally affected in the condensed phase by solvent and supramolecular interactions, can be accomplished through the generation of diastereomeric complexes in the isolated state and their spectroscopic investigation. This review presents a detailed discussion of the mass resolved Resonant Two Photon Ionization (R2PI-TOF) technique in supersonic beams and introduces an overview of various other technologies currently available for the spectroscopic study of gas phase chiral molecules and supramolecular systems. It reports case studies primarily from our recent work using R2PI-TOF methodology for chiral recognition in clusters containing molecules of biological interest. The measurement of absorption spectra, ionization and fragmentation thresholds of diastereomeric clusters by this technique allow the determination of the nature of the intrinsic interactions, which control their formation and which affect their stability and reactivity. *Chirality 21:119–144, 2009.* © 2008 Wiley-Liss, Inc.

*KEY WORDS:* gas-phase clusters; supersonic beam; mass-resolved laser spectroscopy; chiral discrimination; biomolecules

## INTRODUCTION

Understanding molecular recognition phenomena as well as enzymatic catalysis in biological processes requires the knowledge of the structure, the stability, and the dynamics of the molecule/receptor pairs involved. In the last few years, the development of new gas-phase techniques allowed the study of intrinsic interactions in tailor-made molecular clusters mimicking receptor/molecule systems in the isolated state without any interference from the environment.[1–3]

Structure determination is the primary and probably the most important step in the elucidation of the molecular properties of weakly-bound noncovalent clusters. The accurate description of the relative orientation of their components is a daunting challenge for both experimentalists and theoreticians because of the cluster flexibility, which makes their Potential Energy Surface (PES) essentially flat. This feature is essential in molecular recognition

processes and enzymatic catalysis, which are made possible only by facile connections among different PES minima of a molecule/receptor complex. Therefore, molecule/receptor pairs must be regarded as dynamic, rather than as structurally fixed supramolecular systems.

Natural and synthetic receptors are invariably characterized by asymmetric structures with a cavity of appropriate shape and size holding suitable functional groups in specific positions. Their amazing catalytic proficiency and the exceptional selectivity toward biomolecules are ascribed to

a combination of: (i) shape-specific intermolecular interactions between functionalities located on the host/guest complementary surfaces, which severely limit their translational and (overall) rotational motion, and (ii) the rate acceleration due to partial desolvation of the functionalities themselves in the host cavity. Thus, the study of chiral clusters in the gas phase may provide precious information on chiral recognition and rate acceleration of biological processes.

Specifically designed spectroscopic methodologies are generally employed for these purposes. High-resolution laser spectroscopy can provide detailed information on the structure and the conformational equilibria of neutral molecular clusters as well as on the nature of the intervening intracomplex forces. Furthermore, mapping the electronic structure of the ionized clusters may elucidate the influence of some molecular parameters, such as the ionization potentials or ionic reaction thresholds, on many biochemical processes. Finally, cluster mass selection is desirable for studying the variation of the molecular parameters with cluster size and for identifying ionic reactions.

High-resolution laser spectroscopy is facilitated by the generation of cold neutral clusters by supersonic expansion technique.[4] Supramolecular diastereoisomeric complexes can be formed by the association of a selector of precisely defined configuration, e.g., $C_R$, with the R and S enantiomers of a chiral solvent molecule to yield the corresponding $[R•C_R]$ and $[S•C_R]$ diastereomeric adducts. Their structure and energetics can be investigated by Resonant Two Photon Ionization Spectroscopy (R2PI). The species C, denoted as the chromophore, is first promoted from its electronic ground state $S_0$ to the electronic excited state $S_1$ via a resonant absorption step. Then, the absorption of a second photon takes the species into the ionization continuum. Because the ionization cross section is larger for resonant than for nonresonant processes, an increase in the ionization yield of C will be obtained each time the energy $h\nu_1$ excites C from its ground state to a precise vibronic level of $S_1$. If the frequencies of the excitation and ionization photons are equal, the process is named one color R2PI (1cR2PI), otherwise two colors R2PI (2cR2PI) (Fig. 1). The diastereoisomeric $[R•C_R]$ and $[S•C_R]$ complexes can be distinguished through absorption spectra, hole-burning techniques, binding energy measurements, fragmentation thresholds.[5–9] The aim of this review is to present the most recent applications of the R2PI technique as well as other spectroscopic methodologies to the study of chiral clusters in the gas phase.

## EXPERIMENTAL METHODOLOGY

The basic experimental setup for R2PI spectroscopy is shown in Figure 2. It consists of a supersonic molecular beam source, a vacuum system where laser excitation and ionization of the clusters take place, and a time-of-flight (TOF) mass spectrometer for analyzing the formed ionic species. Molecules are premixed in different containers with noble gases and expanded into vacuum through a pulsed nozzle. The containers, inlet line, and nozzle are independently thermostattable. The supersonic jet is colli-

mated by a skimmer and enters into a second chamber where molecules and clusters are ionized by one or two lasers. The ions produced are accelerated by a Wiley–McLaren-type[10] acceleration system and detected by a channeltron or multichannel plate placed at the end of the TOF tube. In a typical two-color experiment, two laser pulses have independently adjustable frequencies for excitation ($\nu_1$) and ionization ($\nu_2$). The wavelengths required by the system are provided by Nd:YAG-pumped pulsed dye lasers with associated crystals for nonlinear optical conversion.

### Resonant Two-Photon Ionization

In a R2PI experiment, a first UV laser photon ($h\nu_1$) excites a specific rovibronic transition of a molecule or cluster and, then, a second UV laser photon of equal ($h\nu_1$) (Fig. 1a) or different frequency ($h\nu_2$) (Fig. 1b) ionizes the excited neutral species. In the first case, we speak of a one-color Resonant Two Photon Ionization (1cR2PI) experiment, whereas we speak of a two-color Resonant Two Photon Ionization (2cR2PI) experiment in the latter case. The formed ions can be readily identified by mass spectrometry. Usually, lasers with pulse duration of few nanoseconds are employed, with typical pulse energies of ≈500 μJ. The absorption of the ionizing photon must be within the lifetime of the excited state populated by the absorption of the first photon. This means that if the excited species exhibit an ultrafast decay into another electronically excited state which the second photon is unable to efficiently ionizes, the method fails, at least in the nanosecond time scale.

If generated in a supersonic beam, molecules and clusters display noncongested 1cR2PI spectra characterized by sharp signals. This comes from the efficient cooling of the translational, rotational, and vibrational degrees of freedom of supersonically expanded species. Only low rotational and vibrational energy levels are populated in their ground-state and their transverse velocity distribution is reduced. Rotationally resolved spectra can be obtained if narrow bandwidth lasers are used.[11–13]

For isolated molecules, the Bolzmann conformer distribution before the expansion may be preserved provided that interconversion barriers between conformers are sufficiently high. The collisional relaxation during the free jet expansion, on the other hand, may partly drain the population into the most stable conformational structures. This is also true for clusters, which are formed and stabilized during the free jet expansion.

The combination of the resonant ionization of cool species with time-of-flight (R2PI-TOF) mass detection makes the methodology very selective (because of the high spectral resolution) and sensitive (because of the efficient ion detection). The possibility to discriminate ions of different sizes present in the beam and detect them simultaneously, allows the analysis of the absorption spectra of all clusters in a single wavelength scan. In general, the absorption spectrum of a monosolvated chromophore (denoted as [solv•C]) differs from that of the unsolvated one (denoted as C) by virtue of the weak intermolecular interactions between chromophore and solvent.
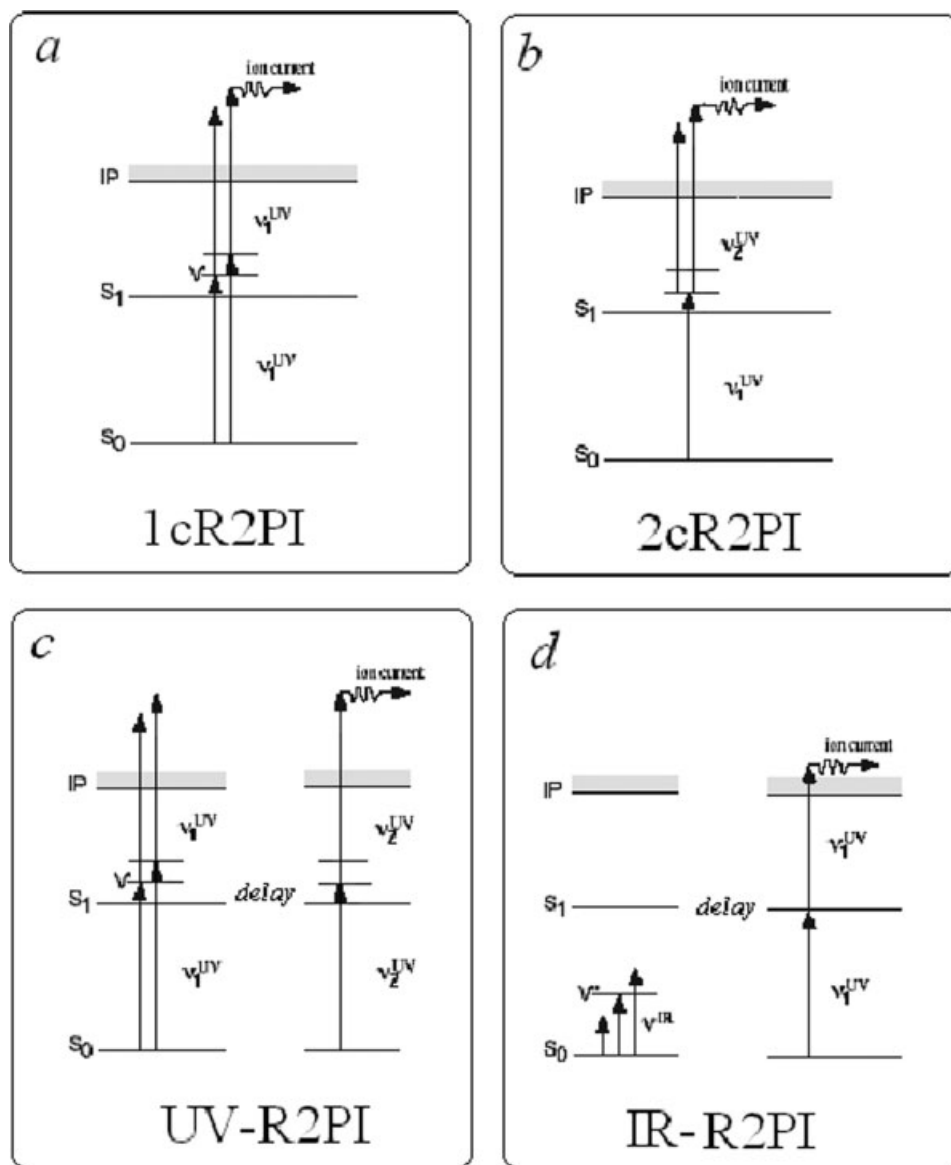
**Fig. 1.** Energy-level diagrams for (**a**) one color Resonant Two Photon Ionization, (**b**) two color Resonant Two Photon Ionization, (**c**) UV-R2PI, and (**d**) IR-R2PI schemes. See the text for further details.

According to the Frank-Condon principle, vertical electronic transitions will alter the chromophore electron charge distribution, but not its internal geometry. Thus, the magnitude and direction of the spectral shift of the chromophore in a cluster arise from the combined effects of the specific structure of the chromophore/solvent complex and of the noncovalent interactions involved. In fact, attractive (dipoles or higher multipoles including hydrogen bond, permanent-induced multipole interactions, dispersion terms) and repulsive (exchange) interactions affect the charge distribution in the ground and excited chromophore which, in turn, depends on polarity and polarizability of the solvent molecule itself. Two opposite situations can be faced: (1) a spectral blue-shift of the $S_1 \leftarrow S_0$ electronic transition in [solv·C] with respect of that in the isolated C ("ipsochromic shift"). The complexation of

the chromophore results in a larger stabilization of the ground state with respect to the excited state and, thus, an increase in the energy difference between the $S_0$ and $S_1$ states; (2) a spectral red-shift of the $S_1 \leftarrow S_0$ electronic transition in [solv·C] with respect of that in the isolated C ("bathochromic shift"). Cluster formation implies a lower stabilization of the ground state with respect to the excited state and, thus, a reduction of the energy difference between the ground and excited state.

The isolated enantiomers S and R of a chiral molecule exhibit the same spectral features because their physical properties (except for weak forces[14–16] which cause enantiomers to differ very slightly in energy) are equivalent. However, their aggregation with a chiral chromophore of defined configuration (e.g., $C_R$) leads to the formation of two diastereomeric complexes with different spectral
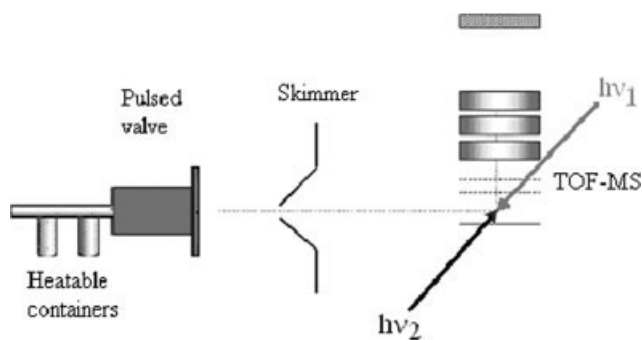
**Fig. 2.** Schematic of an experimental apparatus for R2PI spectroscopy

properties, i.e., [S•$C_R$] and [R•$C_R$]. The 1cR2PI spectroscopy is able to discriminate between S and R by measuring the spectral shift of the diastereomeric [S•$C_R$] and [R•$C_R$] complexes with respect to that of the bare chromophore $C_R$. It is convenient to define the diastereomeric clusters as "homochiral" when the chromophore and the solvent have the same configuration (i.e., [R•$C_R$]), and "heterochiral" in the opposite case (i.e., [S•$C_R$]).

The 2cR2PI method has the advantage that not only the excitation frequency ($h\nu_1$) can be changed, and, thus, the electronic structure of the molecule can be probed, but also the ionization frequency ($h\nu_2$) can be tuned, which allows for a mapping of the electronic structure of the ion. The next sections will illustrate some applications of the R2PI techniques to the study of representative molecular and supramolecular chiral systems, with a particular emphasis on the species which serve as models for biological studies.

### 1cR2PI: Spectral Structures of the Excited State of Molecules and Complexes

A molecule will be ionized if the total energy of the two photons absorbed ($2h\nu_1$) exceeds the ionization energy of the molecule (IE). Efficient ionization requires that the energy of the first photon $h\nu_1$ be resonant with one of the real electronic states in the molecule (resonance enhancement). Thus, the neutral UV-absorption spectrum is transferred to the ion current which can be recorded mass selectively. Scanning $\nu_1$ provides the electronic absorption spectra of molecules and clusters.

Application of the 1cR2PI spectroscopy presents some constraints, mostly due to the fact that the second ionizing photon has the same frequency of the first exciting one. Ionizing the species of interest without extensive fragmentation requires that its excitation energy is at least equal or barely larger than one-half its IE. Otherwise, the ion will be produced with a sizable amount of vibrational energy ($2h\nu_1$-IE) which may cause extensive ion fragmentation and more complicated mass spectra. These fragments keep memory of their parent ions, which means that they have the same rovibrational electronic spectral patterns. This is an important characteristic of the 1cR2PI method, which in turn allows one to study the fragmentation and dissociation processes occurring in molecules

and clusters.[17–19] A further complication in the 1cR2PI spectrum interpretation can occur if the fragmentation efficiency of larger cluster ions is 100%. In this case, the size of the ion precursor cannot be assigned by mass spectrometry. To reduce these drawbacks, it is advisable to employ 2cR2PI (see next section); this allows the reduction of the energy of the ionizing photon and lowers the probability of cluster fragmentation.

Supersonic expansion of the species of interest may give rise to the formation of various isomeric structures, which can hardly be distinguished by 1cR2PI-TOF spectroscopy. This difficulty can be overcome by using 2cR2PI-TOF, IR-R2PI spectroscopies, which are described in the next sections, or the UV-R2PI technique. In UV-R2PI hole-burning spectroscopy (see Fig. 1c), a high-power UV laser pulse is tuned through the spectrum to remove a significant fraction of the ground-state population of different conformations via strong vibronic transitions. A delayed UV probe pulse is fixed to detect a particular absorption of a selected conformer. Any transition that shares its initial level with that used in the probe step appears as a decrease in the signal from the probe laser.[20,21]

### 2cR2PI: Ionization Thresholds, Photodissociation, and Photochemical Reactions

Compared with single photon photoionization, where one ultraviolet photon from either laser[22] or synchrotron sources[23] is utilized, 2cR2PI has the advantage of using two tunable ultraviolet photons to reach the ionization continuum (Fig. 1b). A laser of frequency $\nu_1$ pumps a specific vibronic transition of the molecule or cluster while a second laser is tuned ($\nu_2$) at the ionization/fragmentation thresholds of the ionic species. The two lasers are spatially and temporally fully overlapped; the intensity of the excitation laser is lowered ($\approx 30$ μJ/pulse) in order to minimize one color ionization processes. This combination allows selective discrimination of the different species present in the beam. Because the electronic absorption frequencies of the molecules and clusters are usually well separated, only the ions pertaining to a single excited species are formed in this process.

The 2cR2PI methodology has been employed for determining the ionization, dissociation, and fragmentation thresholds of $R$-1-phenyl-1-propanol ([$\mathbf{P_R}$]) and its monohydrated complex ([$H_2O$•$\mathbf{P_R}$]) (Fig. 3). The energy thresholds were recorded by fixing the energy of the excitation laser ($h\nu_1$) at the electronic origin of the most stable [$\mathbf{P_R}$] ($h\nu_1' = 37{,}618$ cm$^{-1}$) and [$H_2O$•$\mathbf{P_R}$] ($h\nu_1 = 37{,}660$ cm$^{-1}$) isomers, and scanning the $h\nu_2$ energy. Above photoionization, the molecule (Fig. 3a) fragments by homolytic $C_\alpha$-$C_\beta$ bond cleavage and the cluster (Fig. 3b) can either dissociate by loss of a water molecule or give rise to $C_\alpha$-$C_\beta$ fragmentation products. Scheme 1 illustrates the lower energy dissociation paths involved in the ionization of the $S_1$ excited $\mathbf{P_R}$ and [$H_2O$•$\mathbf{P_R}$].

Photoion threshold measurements can provide a measurement of the ionization potentials (IPs) and binding energies of the van der Waals clusters in the ground ($D_0''$), excited ($D_0'$), and ionic ($D_0^+$) state.[7,24,25] In a binary cluster where a chromophere C is bound to a ligand solv,
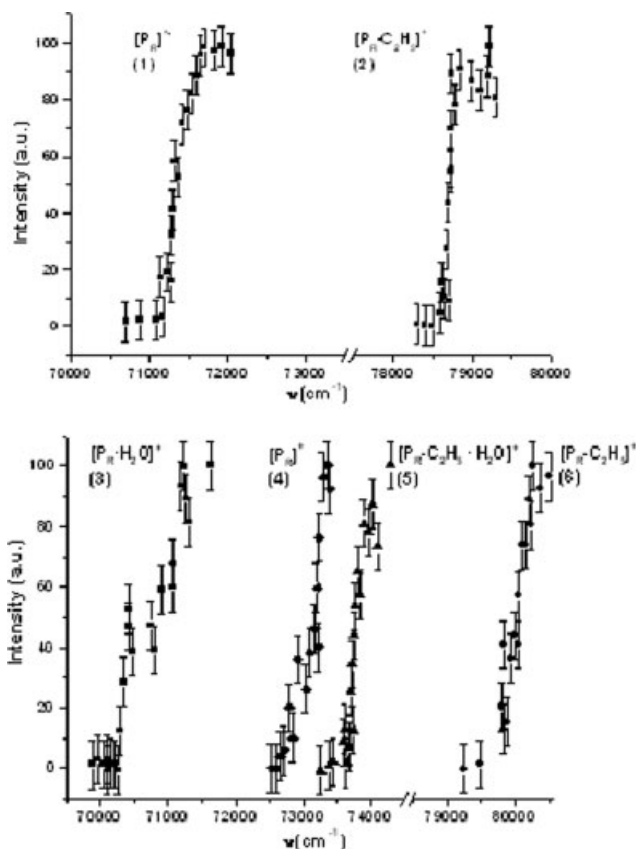
**Fig. 3.** (a) 2c-R2PI appearance thresholds of the $P_R{}^+$ ion and of its ethyl-loss fragment as a function of the total energy ($h\nu_1 + h\nu_2$). The excitation photon $\nu_1$ is fixed at the $0_0^0$ electronic transition of $P_R$ at 37,618 cm$^{-1}$; (b) 2c-R2PI appearance thresholds of the $[P_R \cdot H_2O]^+$ ion and of its fragments as a function of the total energy ($h\nu_1{}' + h\nu_2$). The $\nu_1{}'$ excitation photon is fixed at the $0_0^0$ electronic transition of the $[P_R \cdot H_2O]$ cluster at 37,660 cm$^{-1}$.

the binding energies can be derived from the following relations (see Fig. 4).

$$D_0'' = AE(C^+) - IP(C) \tag{1}$$

$$D_0' = D_0'' - \Delta\nu \tag{2}$$

$$D_0^+ = AE(C^+) - IP([solv \bullet C]) \tag{3}$$
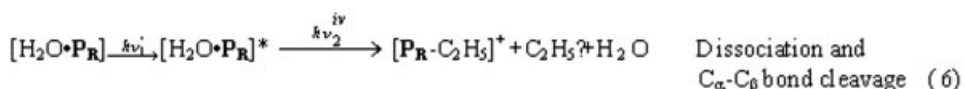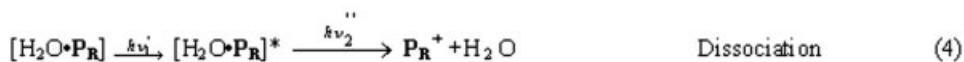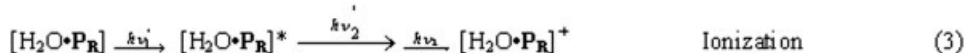
IP(C) and IP([solv·C]) are the measured ionization energies of the chromophore and cluster, respectively, i.e., IP(C) = $h\nu_1$(C*) + $h\nu_2$(C$^+$) and IP([solv·C]) = $h\nu_1{}'$([solv·C*]) + $h\nu_2{}'$([solv·C]$^+$). AE(C$^+$) is the appearance threshold of the ionized chromophore, with excitation step fixed on $S_1 \leftarrow S_0$ transition of the cluster: AE(C$^+$) = $h\nu_1{}'$([solv·C*]) + $h\nu_{2_1}{}''$([C$^+$ + solv]) and $\Delta\nu$ is the shift of the cluster $S_1 \leftarrow S_0$ electronic transition whith respect to the same transition in the bare molecule $\Delta\nu$ = $h\nu_1{}'$([solv·C*]) − $h\nu_1$(C*).

Ionization thresholds and cross sections of clusters have been extensively measured.[7,24–31] In Table 1 the experimental binding energies measured through 2cR2PI in diastereomeric molecular clusters are shown. A general finding is that the ionization energy of molecular clusters ($h\nu_1{}' + h\nu_2{}'$) tends to decrease with its size, the change being more pronounced for smaller clusters. This is mainly due to the extra-stabilization of the ion by the increased polarizability of large clusters. In the case of weakly bound systems, the decreases in ionization energies are found to be considerably larger than the spectral shifts of the electronic transitions. Ionization enhances the intermolecular forces by introducing the influence of a

*Bare chromophore* $P_R$

$$P_R \xrightarrow{h\nu_1} P_R* \xrightarrow{h\nu_2} P_R{}^+ \qquad \text{Ionization} \quad (1)$$

$$P_R \xrightarrow{h\nu_1} P_R* \xrightarrow{h\nu_2'} [P_R\text{-}C_2H_5]^+ + C_2H_5? \qquad C_\alpha\text{-}C_\beta \text{ bond cleavage} \quad (2)$$

*Monohydrated chromophore* $[H_2O \bullet P_R]$

$$[H_2O \bullet P_R] \xrightarrow{h\nu_1'} [H_2O \bullet P_R]* \xrightarrow{h\nu_2'} h\nu_1 \ [H_2O \bullet P_R]^+ \qquad \text{Ionization} \quad (3)$$

$$[H_2O \bullet P_R] \xrightarrow{h\nu_1'} [H_2O \bullet P_R]* \xrightarrow{h\nu_2''} P_R{}^+ + H_2O \qquad \text{Dissociation} \quad (4)$$

$$[H_2O \bullet P_R] \xrightarrow{h\nu_1'} [H_2O \bullet P_R]* \xrightarrow{h\nu_2'''} [H_2O \bullet P_R\text{-}C_2H_5]^+ + C_2H_5? \qquad C_\alpha\text{-}C_\beta \text{ bond cleavage} \quad (5)$$

$$[H_2O \bullet P_R] \xrightarrow{h\nu_1'} [H_2O \bullet P_R]* \xrightarrow{h\nu_2^{iv}} [P_R\text{-}C_2H_5]^+ + C_2H_5? + H_2O \qquad \begin{array}{l}\text{Dissociation and} \\ C_\alpha\text{-}C_\beta \text{ bond cleavage} \quad (6)\end{array}$$

**Scheme 1.** Lower energy paths involved in the 2R2PI process of $P_R$ chromophore and for its binary complex with water $[H_2O \bullet P_R]$.

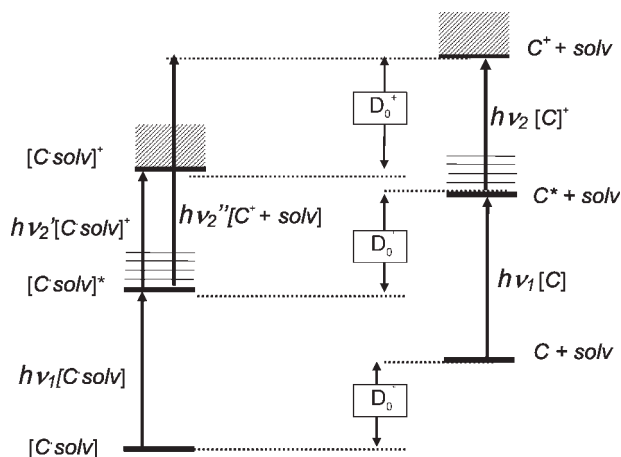**Fig. 4.** Schematic representation of the energy levels of the isolated chromophore (C) and of its complex with solvent (C•solv). $D_0''$, $D_0'$, and $D_0^+$ are the binding energies of the adducts in the ground, excited, and ionized state, respectively.

charged center.[31,32] A consequence of the stronger interactions upon ionization is that the equilibrium geometry of the ionized complex may differ significantly from that of the neutral states. Broadened ionization onsets are frequently attributed to the spectral superposition of ionization into several vibrational levels for which Franck-Condon factors are more favorable.[33] As a result, the adiabatic ionization potential may be considerably lower than the vertical potential, and the observed ionization onsets may occur above the adiabatic potential. In the example reported above, with C = $\mathbf{P_R}$ and solv = $H_2O$, the ionization onset measured for the $\mathbf{P_R}$ molecule (curve 1, Fig. 3a) is quite broad, but nevertheless the cation origin is almost accessible to photoionization and the binding energies of the cluster in the $D_0''$ state was determined to be 20.2 kJ mol$^{-1}$, which agrees with the predicted value.[34] Different behavior is shown for the hydrogen bonded complex with water. The nonadiabatic broad photoionization threshold of the cluster (curve 3 in Fig. 3b) permits only a lower limit determination of the ion binding energy $D_0+$. Sometimes, the vertical ionization energy is even higher than the fragmentation thresholds and this causes extensive fragmentation of the system even at threshold ionization.[35]

In addition to ionization or dissociation, the R2PI ionized molecule or cluster can undergo more or less extensive fragmentations. The fragmentation thresholds can be measured by scanning the energy of the ionizing/fragmenting ($h\nu_2$) photon and looking at the appearance thresholds of the produced ionic fragment (Figs. 3a and

3b). Scheme 1 reports an example of determination of the thresholds for the homolytic $C_\alpha$-$C_\beta$ bond cleavage in $\mathbf{P_R}$ and [$H_2O•\mathbf{P_R}$]. The activation energies can be derived from the relations:

$$E_{act}([\mathbf{P_R}]^+) = AE([\mathbf{P_R} - C_2H_5]^+) - IP(\mathbf{P_R}) \qquad (4)$$

$$E_{act}([H_2O • \mathbf{P_R}]^+) = AE([H_2O • \mathbf{P_R} - C_2H_5]^+) \\ - IP(H_2O • \mathbf{P_R}) \quad (5)$$

where $AE([\mathbf{P_R} - C_2H_5]^+)$ and $AE([H_2O•\mathbf{P_R} - C_2H_5]^+)$ are the appearance thresholds of the fragments resulting from homolytic $C_\alpha$-$C_\beta$ bond cleavage in the ionized molecule and cluster, respectively. $IP(\mathbf{P_R})$ and $IP(H_2O•\mathbf{P_R})$ are the ionization energies of $\mathbf{P_R}$ and ($H_2O•\mathbf{P_R}$).

### IR-R2PI: Conformational Landscapes of Ground State Molecules and Complexes

Infrared R2PI (IR-R2PI) requires a tunable infrared laser, which fires ahead of the UV probe laser. As pointed out above, the spectral bands of molecules and complexes are usually well separated to allow exclusive R2PI ionization of a well-defined species. In general, the UV frequency remains fixed on a specific electronic transition of the cool molecule or cluster, producing an ion signal. When the IR wavelength is scanned ahead the UV laser (Fig. 1d), vibrational transitions are induced by the IR light and the ground state population of the cooled species is depleted. This result in a reduction of the number of ions produced. By measuring the ion signal while tuning the IR wavelength, an ion-dip spectrum is recorded.[36–40] The so-called IR depletion spectrum represents the ground state vibrational spectrum of the probed species. It allows the discrimination of different conformers and to elucidate the size and structure of the ground state species. The distinction of conformers is achieved by selecting the frequency of the UV laser. UV absorption frequencies pertaining to different conformers will display a different IR spectrum. Spectra provide insight into the conformational arrangement, as IR transitions exhibit shifts in absorption frequency and changes in intensity in the presence of, for instance, intra-molecular hydrogen bonds or solvating molecules.

Developed by Lee and coworkers,[36,37] this method was first used by Riehn et al.[38] to investigate intracluster ion–molecule reactions following R2PI. Most of the experiments have been performed employing IR laser systems in the spectral region where the C—H, O—H, N—H, and C=O stretching fundamentals are found, but also exten-

**TABLE 1. Experimental binding energies in diastereomeric molecular complexes**

| Chromophore | Partner | $D_0''$ | $\Delta D_0''$ | Reference |
|---|---|---|---|---|
| (R)-1-phenyl-1-propanol | (S)-2-butanol | $4.8 \pm 0.2$ | 1.1 | 7 |
| (R)-1-phenyl-1-propanol | (R)-2-butanol | $5.9 \pm 02$ | | |
| (R)-1-phenyl-1-propanol | (S)-2-pentanol | $3.1 \pm 0.2$ | 1.6 | 115 |
| (R)-1-phenyl-1-propanol | (R)-2-pentanol | $4.7 \pm 0.2$ | | |
| (R)-1-phenylethanol | (S)-2-butanol | $0.9 \pm 05$ to $1.29 \pm 0.46$ | 1.0–0.71 | 25, 122 |
| (R)-1-phenylethanol | (R)-2-butanol | $1.9 \pm 0.5$ to $2.00 \pm 0.4$ | | |

sion to the mid-IR (fingerprint) spectral region has been achieved by the coupling of R2PI to Free Electron Laser (FEL) radiation.[39] It has been applied to isolated or hydrated chiral molecules but rarely employed for studying clusters of chiral molecules.[9]

### Other Gas Phase Spectroscopic Techniques

Several other spectroscopic techniques have been applied to date for the study of chiral discrimination in the gas phase and should be mentioned here. The first is Laser Induced Fluorescence (LIF) spectroscopy. Electronic absorption spectra of weakly bounded chiral partners were obtained for the first time by the group of Lahmani and coworkers[5] by means of LIF spectroscopy. LIF is based on the electronic excitation of supersonically expanded molecules and clusters by absorption of light quanta from a tunable laser. The excited states may spontaneously release a photon and the emitted fluorescence is collected at right angles to both the excitation laser direction and the beam axis. The fluorescence decay times can also be measured with a photomultiplier.

In the basic experimental configuration, without wavelength dispersion, the spectrum reports the total detected fluorescence versus exciting wavelength. It contains the superimposition of spectra (with absorption coefficients of different magnitudes) of all the species present in the jet. LIF provides the same spectroscopic information on neutral excited states as 1cR2PI, but without the benefit of mass resolution. The applicability of the two UV spectroscopic techniques, LIF or R2PI depends on the electronic structure of the molecule under investigation. LIF spectroscopy is only applicable if the excited state has a sufficiently large quantum yield for fluorescence, whereas R2PI requires that the lifetime of the excited state be as long as the laser pulse duration.

The second spectroscopic technique is jet Fourier Transform Infrared Spectroscopy (FTIR), which allows the detection of vibrational band structures of cooled complexes. Unlike with LIF and R2PI electronic spectroscopies, an aromatic chromophore is not required. Suhm et al. measured the jet FTIR spectra of racemic and enantiopure glycidol dimers and multiple aggregates of lactates.[41,42] The homochiral and heterochiral clusters were distinguished via FTIR spectroscopy and their structure assigned.

The third technique is microwave spectroscopy. With rotational resolution unique structural information about the complexes is obtained, which is difficult to extract from electronic and FTIR spectroscopic investigations. King and Howard[43] reported the first high resolution study of the heterochiral butan-2-ol dimer using a FT microwave (MW) spectrometer. More recently, the rotational spectra of gas phase homo- and heterochiral dimers of propylene oxide have been reported by Xu and coworkers.[44] Several conformers, bound by O•••H—C interactions, were observed and assigned either for the homo- and for the heterochiral dimers.

The fourth technique is circular dichroism in the photoelectron angular distribution (CDAD). In the photoelectron angular distribution, dichroism arises only from the electric dipole operator and, therefore, its magnitude is significantly larger than the conventional CD absorption effects. CDAD effects in randomly oriented (gas phase) chiral molecules were predicted by Ritchie[45] a few decades ago. Gas phase bromocamphor enantiomers were experimentally distinguished for the first time by Bowering et al.[46] Shortly afterwards CDAD effects measured on rigid and floppy[47–50] chiral molecules demonstrate the usefulness of this methodology for highlighting the structural, conformational, and vibrational factors.

Rydberg electron transfer[51] (RET) spectroscopy has also been successfully applied to discriminate the diastereomeric complexes of R-1-phenylethanol with R- and S-2-pyrrolidinmethanol (prolinol) (Lecomte et al., 2005, private communication). Finally, very small energy differences between enantiomers are predicted due to symmetry breaking by weak interactions.[14–16]

### Computational Methodologies

Gas phase studies enjoy a unique synergism between theory and experiment. Isolated molecules and clusters are the exact replica of the theoretical model system. A large amount of experimental data which has been obtained from the methodologies described in this review can be used by theoretical chemists as benchmark for the validation of model potentials of ab initio calculations.

A wide number of theoretical approaches have been employed to study complexes formed by chiral molecules. These methods include classical and quantum numerical simulations. Classical molecular dynamic and Monte-Carlo Docking calculations,[52–56] based on standard force fields, have been used especially to investigate conformational issues. Quantum approaches have generally been employed to carry out ab initio calculations of more or less higher accuracy, depending on the size of the basis set. Most commonly used is the supermolecular variational method which computes the interaction energy as the difference between the energy of the cluster and the energy of the isolated systems. A clear overview of the structures, vibrational frequencies, and interaction energies has been obtained at different levels of theory: Hartree-Fock, and electron correlation Hamiltonians, such as density functionals, Moller-Plesset, and coupled-cluster methods.[57–62] The supermolecular approach is generally corrected for the basis set superposition error with the counterpoise method. This can be applied after the geometrical optimization or, with a higher computational effort, during the optimization itself.

Recently, a new approach[63] based on ab initio multiconfiguration method and on the BSSE-Counterpoise allowed us to reproduce the shift of the electronic transitions in clusters with respect to the electronic transition in isolated molecules. This procedure could help in assigning experimental spectral features to specific conformation of the molecular adduct. The quantal results can be analyzed with respect to the electrostatic and polarization forces and electron-density differences. Then, they are analyzed with respect to the shifts of the electronic transitions.

The energy range associated with these spectral shifts rarely exceeds a few hundred wavenumbers and, there-

fore, falls well within the computation uncertainty of the most common ab initio methodologies. Hartree Fock methods such as Moller-Plesset *n*th order and Configuration Interactions techniques or Time-dependent Density Functional Theory were applied to study single aromatic molecules[64–67] and their adducts with rare-gas atoms or small organic molecules.[68–71]

The new approach treats in a consistent way both the $\pi$ and $\pi^\star$ electronic states of both chromophores and their molecular adducts. Their correct energy gaps are obtained by forcing the computational errors to be systematic in the two electronic states of the chromophore molecule and of their molecular adducts. This set has been accomplished by expanding the wavefunctions of the chromophores and molecular adducts over the same set of Gaussians; this set is formed by Gaussians centered on the nuclei of the chromophore and on the nuclei of the solvent molecules.

A new basis set has been formed by standard Slater Type Gaussian Orbitals (STO-6G) together with a subset of conventional Pople Gaussians. The Complete Active Space Self Consistent Field (CASSCF) procedure was employed because it provides a correct description of both the ground and excited electronic states.[72–74] The electronic excited $\pi^\star$ states are constrained to be open shell spin singlet states in order to correctly represent the configuration of the final states of the electronic transitions.

The active space of the multiconfigurational wavefunctions takes into account the molecular orbitals involved in the excitation process: the three $\pi$ bonding and the three anti-bonding $\pi^\star$ orbitals. In the CASSCF, the six electrons of the lower $\pi$ MOs: CAS(6,6) were included. The basis sets used for the molecular adducts were taken by mixing two different types of atomic orbitals: the occupied shells were represented with Slater Type orbitals each fitted with six Gaussian functions (STO-6G); the virtual shells were taken from the Pople standard basis set 6-31G**. This scheme was chosen because Slater type functions diffuses more than the Pople orbitals, are expected to better account for the need of a $\pi$ diffuse space over the aromatic plane. To overcome the well-known deficiencies of the STO-6G when it comes to properly describing weak intermolecular interactions, the Pople part of the basis set was chosen.

### Chiral Molecules in the Gas Phase

Enantiomers can be discriminated by interaction with either circularly-polarized light (CPL) or chiral molecules. Very recently, resonance-enhanced multiphoton ionization circular dichroism (REMPI-CD) has been employed to discriminate gas phase 3-methylcyclopentanone enantiomers, either in nozzle-jet expanded[75] or in effusive[76] molecular beams. Circular dichroism (CD) is defined as the differential absorption for *levogyric* (*l*-CPL) and *dextrogyric* (*d*-CPL) circularly polarized light by optically active molecules. In these experiments,[75,76] a differential ionization efficiency is observed in *l*- and *d*-CPL-induced multiphoton ionization process of the isolated enantiomers of 3-methylcyclopentanone. The gas phase REMPI-CD methodology may provide information on the absolute configuration of bare

chiral molecules and can be regarded as a useful complementary alternative to the REMPI methods.

The R2PI approach to chiral discrimination in supersonic beams is based on the formation of molecular diastereomers as described in the previous sections. Although no information on the absolute configuration of isolated chiral molecules can be obtained by the R2PI techniques, their application may offer evident advantages. Indeed, large chiral molecules of biological or pharmaceutical interest are often relatively floppy which, in their electronic ground state, may reside in several PES minima corresponding to various quasi-degenerate conformational structures. These properties are at the basis of the physiological behavior of biomolecules because they can interact with receptors though a reciprocal (and reversible) modification of their structures. Therefore, the knowledge of the structure and the conformational landscape of biologically relevant isolated molecules (and of their modification in noncovalent complexes) is a prerequisite for understanding their selectivity, function, and, ultimately, physiological activity.

Precious structural information has been gathered on biologically relevant chiral molecules, such as neurotransmitters,[35,77–80] amino acids,[81,82] small peptides,[83–88] and sugars,[89–92] by the use of the R2PI, IR-R2PI, and UV-R2PI spectroscopies. The same techniques have been employed for investigating the structure and the conformational behavior of covalently bound diastereoisomers. Simons and coworkers[79] studied the neurotransmitter ephedrine and its diastereoisomer pseudoephedrine. De Vries and coworkers[83] reported a R2PI study of the structural differences of covalently bonded diastereomeric pairs of L-Phe-L-Phe and L-Phe-D-Phe and of L-Val-L-Phe and D-Val-L-Phe. Recently Mons and coworkers[93] investigated intramolecular chiral recognition by R2PI and IR-R2PI in capped dipeptides, namely Ac-L-Ala-L-Phe-NH$_2$, Ac-D-Ala-L-Phe-NH$_2$.

Also the ionization energy IE of an isolated molecule may depend on its conformation. For instance, the IEs difference is very large for phenylalanine conformers, ranging from 8.80 to 9.15 eV.[94] Two distinct subgroups of the six lowest energy conformers of Phe have been identified on the basis of the magnitude of IEs. In a recent study, the structural and electronic properties of L-Phe ion conformers were also investigated by subsequent dissociation of the cation formed in a R2PI process.[95]

### Supramolecular Complexes of Chiral Molecules with Achiral Solvents

All the studies reported in the previous section concern isolated molecular systems in the absence of solvent. In nature, biologically relevant molecules establish hydrogen-bonding and Van der Waals interactions with other species. The preference of a solvent molecule for certain binding sites of a solute molecule is a problem of general interest and cluster studies provide valuable insights into the relative importance of specific interactions. Water is the solvent of excellence in living systems; most biomolecules have the capability to form strong hydrogen bonds with water. The study of tailor-made microhydrated systems is of extreme interest, because it can provide pre-
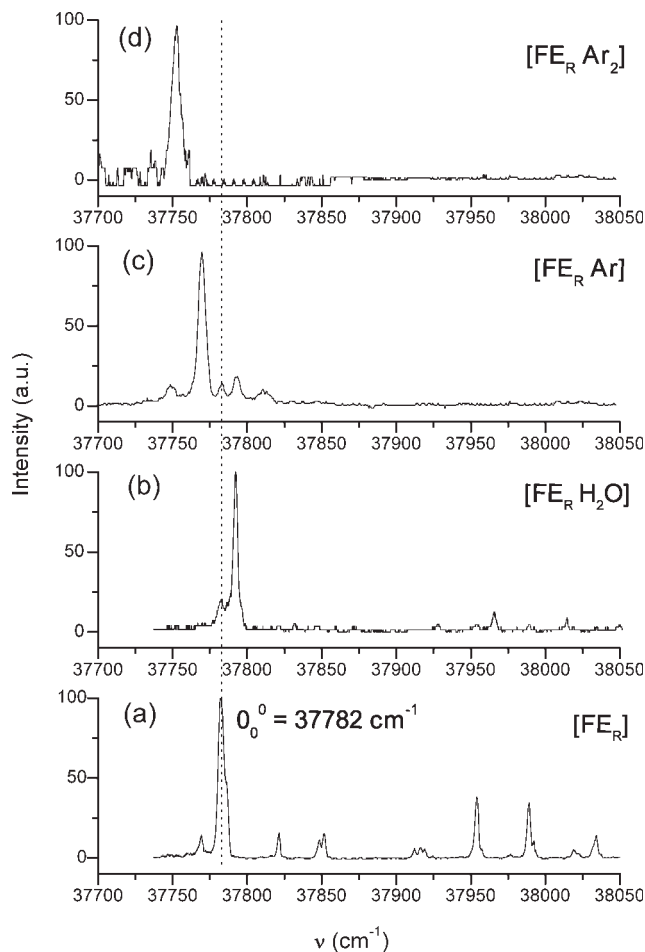
**Fig. 5.** Mass resolved 1cR2PI excitation spectrum of: (**a**) **FE$_R$** molecule measured at $m/z = 176$; (**b**) **FE$_R$•**H$_2$O cluster measured at $m/z = 194$; (**c**) **FE$_R$•**Ar cluster measured at $m/z = 216$; (**d**) **FE$_R$•**Ar$_2$ cluster measured at $m/z = 256$. The dashed line refers to the $0_0^0$ electronic origin of the S$_1$←S$_0$ transitions of the most stable **FE$_R$** conformer (37,782 cm$^{-1}$).

this field. Here, some recent results from our work are presented regarding a fluorinated aromatic chiral chomophore, i.e., *R*-1-phenyl-2,2,2-trifluoroethanol (**FE$_R$**).

### Microsolvation Effects on R-1-Phenyl-2,2,2-trifluoroethanol (FE$_R$)

The replacement of a hydrogen atom by a fluorine atom is a strategy widely used in drug design to alter biological function. Fluorine is introduced to block a metabolically labile site in the molecule, to modulate its physicochemical properties, and to increase its binding affinity by exploiting specific interactions with the receptor. Fluorine substitution of a hydrogen atom does not typically present a major steric perturbation. However, because of the inductive and mesomeric properties of fluorine, the biological response to the fluorinated compound may change drastically. A fluorine atom may act as a hydrogen bond acceptor and, therefore, the fluorinated molecule may possess particular affinity for enzyme receptors.[99] A large number of therapeutic and diagnostic agents contain strategically placed fluorine atoms. Their importance in biological functions is apparent from the structure of their complexes with the enzymes and drugs,[100] in which the noncovalent interactions play an important role. The structure and the electronic spectra of simple adducts of a chiral fluoroalcohol, i.e., *R*-1-phenyl-2,2,2-trifluoroethanol (**FE$_R$**), with argon[101] and water (**W**)[102] were first investigated by us. The results were compared with those obtained for the nonfluorinated analogue, *R*-1-phenylethanol (**E$_R$**). Two important aspects emerge from this study: the capability of the fluorine atom to act as a hydrogen bond acceptor and the role of the dissymmetric HOCHCF$_3$ substituent in the modification of the π electron density in the ground and excited states of the chromophore.

Figure 5 shows the 1cR2PI spectra recorded at the mass of the **FE$_R$**, [**W•FE$_R$**], and [Ar$_n$•**FE$_R$**] ($n = 1,2$) complexes, in the frequency range of the $0_0^0$ electronic transition. All four spectra display a very intense band, which is the most red shifted band (apart from some small peaks that are clearly attributed to the fragmentation of [Ar$_n$•**FE$_R$**] ($n = 1,2$) clusters).

Three structures have been recognized on the HF/6-31G calculated potential energy surface of **FE$_R$**, and are reported in Figure 6 together with the relative energies calculated at MP2/6-31G** level of theory. The most stable conformer **I** is characterized by the OH group located out of the plane of the phenyl ring, which establishes an intramolecular hydrogen bond with the fluorine atom of

cious information the influence of this ubiquitous biological solvent. Indeed, some important aspects of the behavior in aqueous solution may be mainly due to a few first-shell water molecules interacting with functional groups and can be clarified by the spectroscopy of the gas-phase complexes.

Studies on the effects of microsolvation on chiral and achiral molecules are reported in several reviews,[30,96–98] which highlight the impact of the R2PI spectroscopy in



**Fig. 6.** MP2/6-31G** optimized structures and relative energies of the three most stable conformers of **FE$_R$**.
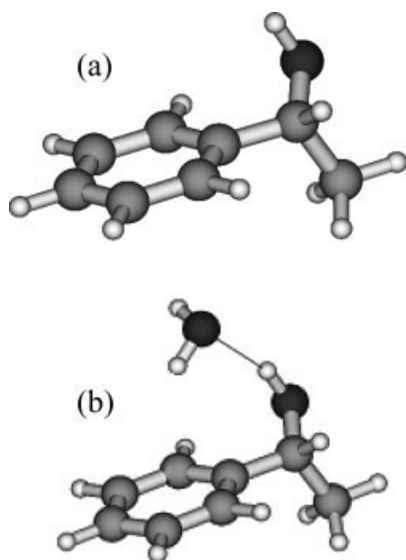
**Fig. 7.** Ab initio B3LYP/6-31G** calculated structures for (**a**) *R*-(+)-1-phenylethanol and (**b**) the adduct with $H_2O$ of *R*-(+)-1-phenylethanol.



**Fig. 8.** Ionization potential threshold of **FE$_R$**. Inset: MP2/6-31G** optimized structure of ionic state of the bare chromophore.

the CF$_3$ group *anti* to the phenyl ring. Conformer **II** is similar to the most stable conformer of *R*-1-phenylethanol **E$_R$** (Fig. 7a) with the hydroxyl hydrogen atom pointing toward the ring plane (OH•••π bonding). The conformational barrier between **I** and **II** is estimated as large as 9.6 kJ mol$^{-1}$, and the barrier between **II** and **III** amounts to 3.5 kJ mol$^{-1}$. As a consequence, in the supersonic expansion of the **FE$_R$** molecule, conformer **I** presumably predominates relative to the other conformers. Therefore, the intense band at 37,782 cm$^{-1}$ in the spectrum of **FE$_R$** (Fig. 5a) can be assigned to the $0_0^0$ electronic $S_1 \leftarrow S_0$ transition of the most stable molecular conformer **I**. Differing from the analogous **E$_R$** molecule (Fig. 7a), the presence of the CF$_3$ group in **FE$_R$** induces the formation of an intra OH•••F hydrogen bond. The experimental ionization energy of **FE$_R$** and the stiffness of the ionization threshold (Fig. 8) supports this assignment. In fact, the structure of the **FE$_R$$^{•+}$** ion (inset of Fig. 8) resembles that of the ground-state neutral conformer **I** and the measured ionization energy (9.22 eV) is in agreement with the theoretical value of 9.02 eV calculated at the MP2/6-31G** level of theory.

The B3LYP/6-31G** search of energy minima for the [**W•FE$_R$**] complex is characterized by the presence of three structures differing in the conformation of the chro-
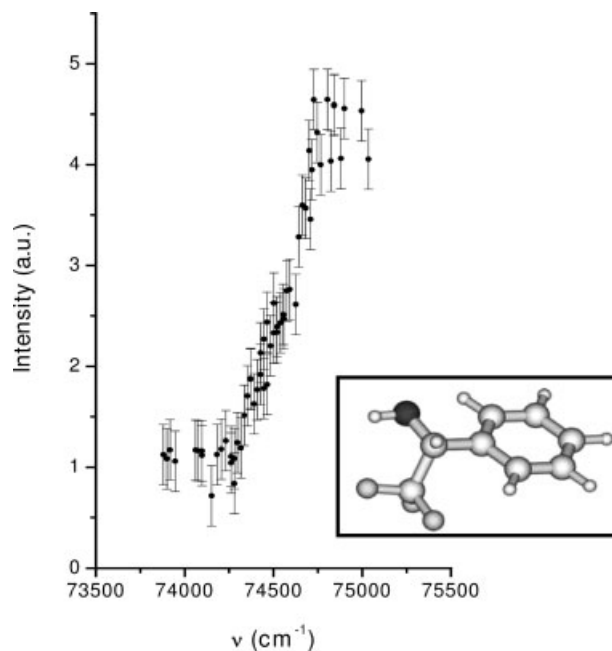
mophore and the specific interaction with the solvent (Fig. 9). In the most stable structural conformer **A**, the water molecule acts as a proton acceptor from the **O**H group of the chromophore (the oxygen atom of alcoholic chromophores is henceforth denoted in boldface) and as a proton donor toward the F atom *anti* to the aromatic ring. In conformer **B**, the water molecule acts as a proton acceptor from the **O**H group of the chromophore and as a proton donor toward its π-ring. In the least stable structure **C**, the water molecule acts as a proton acceptor from the **O**H group of the chromophore and as a proton donor toward its F–C$_\beta$ bond quasi coplanar to the aromatic ring. The intense band at 37,782 cm$^{-1}$ in the spectrum of [**W•FE$_R$**] (Fig. 5b), can be assigned to the $0_0^0$ $S_1 \leftarrow S_0$ electronic transition of the most stable conformer **A** (Fig. 9). This assignment is supported by the limited value of the blue shift of the $S_1 \leftarrow S_0$ electronic transition (10 cm$^{-1}$) of [**W•FE$_R$**] with respect to the same transition in the bare molecule. Indeed, while the least stable structure **C** can be safely excluded, a different shift is expected for the **B** structure, due to the presence of an OH•••π interaction. It should be
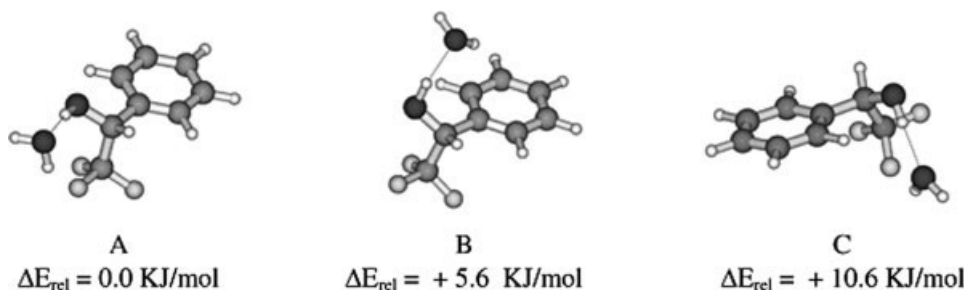


| A | B | C |
|---|---|---|
| $\Delta E_{rel} = 0.0$ KJ/mol | $\Delta E_{rel} = +5.6$ KJ/mol | $\Delta E_{rel} = +10.6$ KJ/mol |

**Fig. 9.** B3LYP/6-31G** calculated structures and relative energies of the three most stable [**FE$_R$•H$_2$O**] complexes.

**Fig. 10.** Ab initio calculated structures and bond dissociation energies ($D_{a,b}''$) of ground-state $[\mathbf{FE_R}^\bullet(\mathrm{Ar})_n]$ ($n$ = 1,2) complexes. The calculations have been performed taking into account the Counterpoise correction to the BSSE.

noted that CASSCF studies predict a blue shift of $+19$ cm$^{-1}$ for structure **A** and about $+4$ cm$^{-1}$ for structure **B** relative to conformer **I**. In the preferred **A** conformation of $[\mathbf{W\cdot FE_R}]$, the water molecule replaces the intramolecular interaction O-H•••F hydrogen bond by two intermolecular **O**H•••O$^w$ and O$^w$-H•••F hydrogen bonds (O$^W$ is the oxygen of water). In the analogous $[\mathbf{W\cdot E_R}]$ cluster,[103] only one stable conformer is detected in the supersonic beam, with the electronic origin shifted by $+54$ cm$^{-1}$ from the electronic origin of the isolated chromophore. In this cluster, O—H•••F hydrogen bonds are obviously absent. The $+54$ cm$^{-1}$ blue-shifted band origin is indicative of O$^w$H•••$\pi$ interaction between water and $\mathbf{E_R}$.[103,104] Accordingly, B3LYP/6-31G** optimized structures predict that in the most stable structure (Fig. 7b), water acts as a proton acceptor from the **O**H group of the chromophore and as a proton donor toward its $\pi$-ring. Similar interactions are present in the less stable conformer **B** of $[\mathbf{W\cdot FE_R}]$. The competition between weak O$^w$-H•••F and O$^w$-H•••$\pi$ hydrogen bond interactions has been studied also in the 4-fluorostyrene–H$_2$O cluster.[105,106] It was shown that the electron attracting effect of fluorine dominates over the releasing mesomeric effect of the vinyl group and, thus, the O$^w$—H•••F interaction is favored over the O$^w$—H•••$\pi$ one. In conclusion, the comparison between the spectral features of $\mathbf{E_R}$ and $\mathbf{FE_R}$, and their monohydrated clusters, shows that in both the bare $\mathbf{FE_R}$ molecule and its $[\mathbf{W\cdot FE_R}]$ cluster, the presence of fluorine prevents $\pi$-type hydrogen bonding with the aromatic ring, which is instead

an important interaction in the analogous $\mathbf{E_R}$ and $[\mathbf{W\cdot E_R}]$ species.

Concerning the $[\mathrm{Ar}_n\mathbf{\cdot FE_R}]$ ($n$ = 1,2) clusters, the relatively small excess energy ($\Delta E = 2h\nu - \mathrm{IE} \sim 0.15$ eV), imparted to them in the 1cR2PI ionization, enables us to observe their unfragmented $[\mathrm{Ar}_n\mathbf{\cdot FE_R}]^{\bullet+}$ ($n$ = 1,2) radical ions in the mass spectrum and to measure their excitation spectra. The ab initio calculated structures and bond dissociation energies ($D_{a,b}''$) of the ground-state $[\mathrm{Ar}_n\mathbf{\cdot FE_R}]$ ($n$ = 1,2) complexes are reported in Figure 10.

It is worth noting that two unequivalent binding sites on the two $\pi$-faces of $\mathbf{FE_R}$ exist for the argon atom. In the most stable $[\mathrm{Ar}\mathbf{\cdot FE_R}]$ adduct, the argon atom is placed above the $\pi$-orbital of the aromatic ring on the face *syn* to the CF$_3$ group ($[1/0]_{up}$ in Fig. 10) while the isomer in which the argon atom is placed on the face *anti* to the CF$_3$ group is slightly less stable. The most stable $[\mathrm{Ar}_2\mathbf{\cdot FE_R}]$ isomer has the two Ar atoms placed on opposite sides of the arene ring (1/1 in Fig. 10), as generally found in aromatic$\cdot$(Rg)$_2$ adducts (Rg = rare gas). The CAS(6,6)/Slater$^+$-calculated $\pi$-electron density difference in the most stable $[1,0]_{up}$ (a), $[1,0]_{down}$ (b), and $[1,1]$ clusters and the predicted shifts are reported in Figure 11. These results show that the dissymmetry induced by the CHOHCF$_3$ substituent on the two $\pi$-faces of the aromatic ring leads to different changes in the shape of $\pi$- and $\pi^*$ electron densities of $\mathbf{FE_R}$ interacting with argon atoms placed on the opposite faces of the aromatic ring. The different shifts of the electronic transitions predicted for the two isomers of

$$\Delta v_{1,0}{}^{th} = -15 \text{ cm}^{-1} \qquad \Delta v_{1,0}{}^{th} = -24 \text{ cm}^{-1} \qquad \Delta v_{1,1}{}^{th} = -31 \text{ cm}^{-1}$$
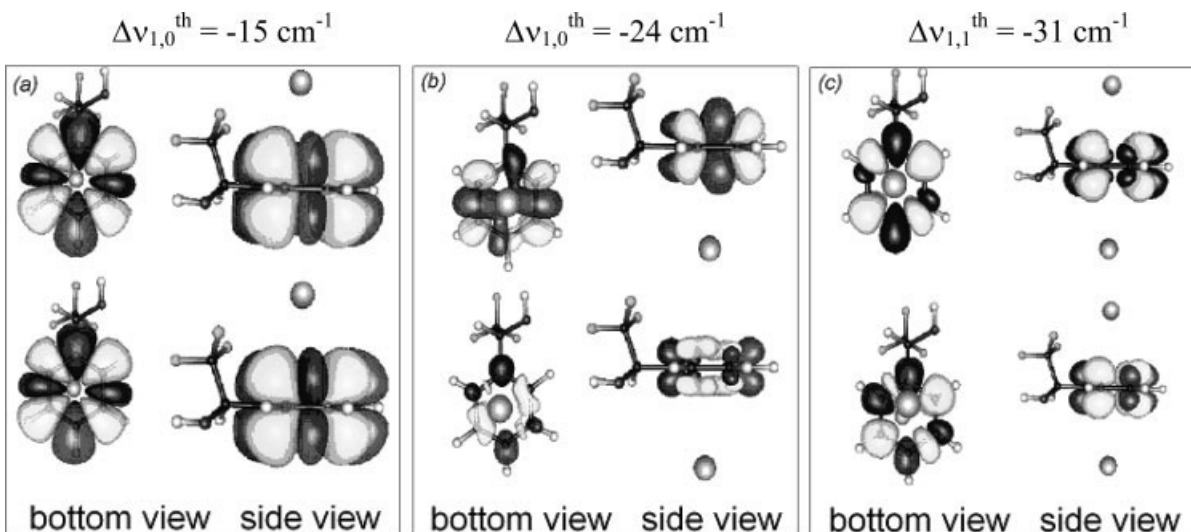


**Fig. 11.** CAS(6,6)/Slater$^+$-calculated $\pi$-electron density difference in the most stable (**a**) $[1,0]_{up}$, (**b**) $[1,0]_{down}$, and (**c**) $[1,1]$ structures of $[\mathbf{FE_R} \cdot (Ar)_n]$ ($n = 1,2$) complexes (top, excited state; bottom, ground state). The regions in colour indicate a change of $5 \times 10^{-4}$ $\pi$-electron density (blue: $+5 \times 10^{-4}$; yellow: $-5 \times 10^{-4}$). The Ar atoms are denoted as pink spheres. CAS(6,6)/Slater$^+$-calculated spectral shift $\Delta v_{a,b}$ in cm$^{-1}$.

$[Ar \cdot \mathbf{FE_R}]$, $[1,0]_{up}$ and $[1,0]_{down}$ (Fig. 10), reflect the different dipole and quadrupole momenta induced in the rare gas atoms by interaction with the opposite $\pi$-faces of the chiral arene itself.

The intense bands in the spectra of $[Ar \cdot \mathbf{FE_R}]$ and $[Ar_2 \cdot \mathbf{FE_R}]$ clusters are consistent with the predominant formation of a single isomeric structure in each case. The shifts of the electronic transitions for the most stable isomers of $[Ar \cdot \mathbf{FE_R}]$ and $[Ar_2 \cdot \mathbf{FE_R}]$ with respect to the same transition in the bare molecule are of $-13$ and $-33$ cm$^{-1}$, respectively. Comparison between the $\Delta v_{1,2}^{th} = -15$ cm$^{-1}$ red shift value, calculated for the most stable $[1,0]_{up}$ $[Ar \cdot \mathbf{FE_R}]$ structure and the $\Delta v_{1,0}^{exp} = -13$ cm$^{-1}$ value, measured for $[Ar \cdot \mathbf{FE_R}]$ (Fig. 5c) enables us to assign this band to the $[1,0]_{up}$ structure. Incidentally, the absence in the $[Ar \cdot \mathbf{FE_R}]$ absorption spectrum of a band red-shifted by $-24$ cm$^{-1}$ relative to the $0_0^0$ electronic $S_1 \leftarrow S_0$ transition of bare $\mathbf{FE_R}$ suggests that the less stable $[1,0]_{down}$ $[Ar \cdot \mathbf{FE_R}]$ structure is not formed in the supersonic beam. The shift measured for $[Ar_2 \cdot \mathbf{FE_R}]$ complex (33 cm$^{-1}$, Fig. 5d) supports the view that the two argon atoms lie on opposite faces of the aromatic ring. The two Ar atoms in $[1,1]$ $[Ar_2 \cdot \mathbf{FE_R}]$ are polarized along different directions because of the influence of the $CF_3$ group on the face *syn* to the $CF_3$ group and of the combined effects of the H and **OH** moieties on the *anti* one. This leads to a change in the shape of $\pi$- and $\pi^*$-electron densities which can be thought of as the sum of the effects of the $[1,0]_{up}$ and $[1,0]_{down}$ plus a small three-body contribution. No additive effects are obviously expected for the conceivable $[2,0]$ $[Ar_2 \cdot \mathbf{FE_R}]$ structure (Fig. 10) owing to the mutual interaction between the two Ar atoms sitting on the same $\pi$-face of the chromophore.

The above results can be compared with the general behavior of other aromatic $\cdot (Ar)_2$ adducts.[107–114] Here, the most stable $[1,1]$ isomer invariably predominates at the su-

personic beam temperature. The two argon atoms interact with the aromatic ring in the same way as in the monosolvated $[1,0]$ complex. This leads always to a $S_1 \leftarrow S_0$ transition red shift $[1,1]$ twice as large as in $[1,0]$. This behavior can be observed also with aromatics containing inherently dissymmetric substituents,[101] such as *R*-2-(*p*-fluoro-phenyl)butane, *R*-2-(*m*-fluoro-phenyl)butane, or wherein both sides of the aromatic plane are nonequivalent, as in the pyramidal structure of aniline.[112]

The spectral shift measured for the $[1,1]$ isomer of $[Ar_2 \cdot \mathbf{FE_R}]$ (33 cm$^{-1}$) is not twice as large as that measured for the $[1,0]$ $[Ar \cdot \mathbf{FE_R}]$ complex. Indeed, it is much larger ($\Delta v_{1,1}/2\Delta v_{1,0} = 1.27$). Differently from most investigated aromatic $\cdot (Ar)_2$ adducts, the two $\pi$ faces of $[Ar \cdot \mathbf{FE_R}]$ and $[Ar_2 \cdot \mathbf{FE_R}]$ feel the effects of chemical groups with remarkably different electronic properties ($CF_3$ and **OH**). The opposite net charge distribution on these groups induces an appreciable asymmetry in the $\pi$-electron density of bare $\mathbf{FE_R}$ in both the $S_0$ and $S_1$ states, which is differently perturbed by interaction with the Ar atoms. This observable effect is even greater for the more polarizable Kr complex with $\mathbf{FE_R}$ ($\Delta v_{1,1}/2\Delta v_{1,0} = 1.36$).[101]

### Supramolecular Diastereomers

As pointed out above, the *R*- and *S*-enantiomers of a chiral molecule can be discriminated in the gas phase by complexation with another chiral molecule of precisely defined configuration. Enantiomers interact in a different manner with a chiral molecule and their noncovalent homo and heterochiral complexes are no longer mirror images, i.e., they have different physical and chemical properties which can be spectroscopically investigated by the R2PI methodology. R2PI spectroscopy of diastereomeric clusters has been employed in the past, mainly by our group, to study the spectroscopic properties and the interaction energies in hydrogen bonded clusters of sev-
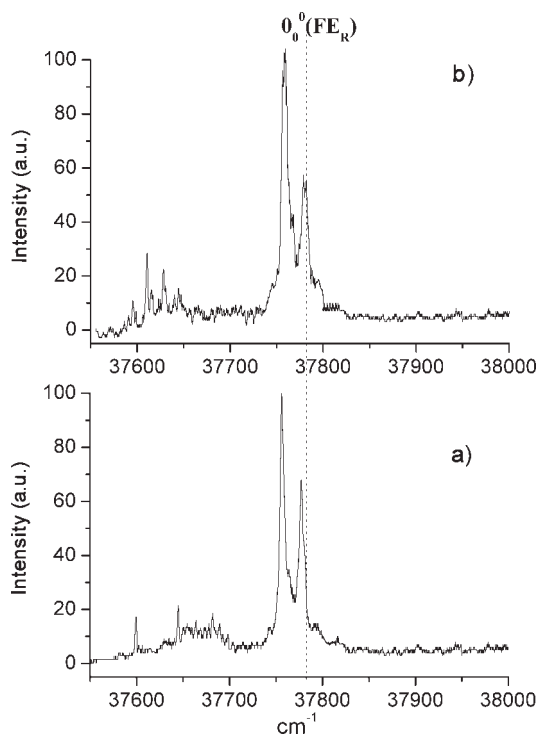
**Fig. 12.** 1cR2PI excitation spectra of the complexes between $FE_R$ and (a) $A_R$, (b) $A_S$. The dotted line refers to the $0_0^0$ transition for the most stable conformer **I** of the bare chromophore $FE_R$.

eral chiral aromatic alcohols (cromophores) bonded to a variety of solvent molecules, including chiral mono and bifunctional alcohols, amines, and water.[115–117] The shifts of the electronic transitions, excited state vibrational frequencies, binding energies, and activation barriers of these complexes were determined, showing their sensitivity to the chirality of their components. More recently, we focused our attention on the study of chiral molecules of biological or pharmaceutical interest, or tailor-made complexes containing components which mimic the building blocks of large biomolecules. More specifically, we investigated the effects of inter- and intramolecular interactions in the structure and spectral properties of complexes containing chiral fluoroaromatics,[118] furanose rings analogues,[119,120] esters,[121] and neurotransmitters.[80]

### *The Effect of Fluorine Substitution on Chiral Recognition R-1-Phenylethanol ($E_R$) and R-1-Phenyl-2,2,2-trifluoroethanol ($FE_R$) of R- and S-2-Aminobutane*

To investigate the role of fluorine substitution in the chiral recognition process, we investigated the structure and the vibronic spectra of the adducts of $FE_R$ with R- and S-2-aminobutane ($A_{R/S}$) and compared them with previous results[122,123] obtained for complexes of its nonfluorinated analogues.

A common behavior is observed in the 1cR2PI photoprocess of $FE_R \cdot A_{R/S}$ and $E_R \cdot A_{R/S}$ adducts: in their mass spectra[118,122] the $[PhCHOH \cdot A_{R/S}]^+$ and $[A_{R/S} \cdot H]^+$) ions are observed. The $[PhCHOH \cdot A_{R/S}]^+$ ion is due to homolitic $C_\alpha$-$C_\beta$ bond fragmentation with the corresponding $CF_3$

or $CH_3$ radical loss; the presence of the $[A_{R/S} \cdot H]^+$ ion indicates the occurrence of a dissociative proton transfer reaction from the ionized chromophore to the $A_{R/S}$ base.

The 1cR2PI excitation spectra of homochiral $FE_R \cdot A_R$ and heterochiral $FE_R \cdot A_S$ clusters are shown in Figures 12a and 12b, respectively. Similar spectra have been recorded at $m/z$ 180 $[PhCHOH \cdot A_{R/S}]^+$ and 74 ($[A_{R/S} \cdot H]^+$), indicating that these fragments derive from a common precursor. The spectra are characterized by very intense peaks in the region of the $0_0^0$ electronic transition of the isolated molecule (marked with a dotted line in Fig. 12) and by some less intense, more red shifted bands. The difference in the spectral shifts of the most intense bands ($\Delta\Delta\nu = \Delta\nu_{homo} - \Delta\nu_{hetero}$) is only $-2$ cm$^{-1}$. In contrast, both $E_R \cdot A_R$ and $E_R \cdot A_S$ display[122] several intense, significantly red shifted bands. Moreover, the difference of the spectral red-shifts of their homo- and heterochiral clusters, $\Delta\Delta\nu = \Delta\nu_{homo} - \Delta\nu_{hetero}$, is 17 cm$^{-1}$.

The B3LYP/6-31G**-calculated potential energy surfaces of the diastereomeric $[FE_R \cdot A_{R/S}]$ complexes reveals the presence of four lowest-energy structures for each diastereomer differing in the conformation of the chromophore and the specific interaction with the solvent (Fig. 13). Analysis of the structural features of the most stable conformers **A** and **B** allows their identification as responsible for pronounced bands of Figure 12. Indeed, the limited spectral shifts of these bands are consistent with the dual function of the $NH_2$ group of amine both as H-bond acceptor from the OH of $FE_R$ and as H-bond donor to the F atom. This dual function, as well as the limited dispersive interactions between the $FE_R$ aromatic ring and the distant amine, suggests that the π-electron densities of the ground and excited state of $FE_R$ are not differently perturbed by the presence of the amine.

The less intense, red-shifted bands in the $FE_R \cdot A_{R/S}$ spectra (Fig. 12) are attributed to the calculated C and D structures, both characterized by the H-bond donating character of the OH group of $FE_R$ toward the amine. In these structures, the amine moiety lies over the aromatic ring of the chromophore.

The structures of the most stable $E_R \cdot A_{R/S}$ clusters are analogues to the C and D structures of $FE_R \cdot A_{R/S}$, with the amine molecule acting as a proton acceptor from the OH group of the chromophore and lying over its aromatic ring. In these structures, O—H•••N hydrogen bonding and dispersive forces with the π-system are the two major interactions stabilizing the adducts. The magnitude of the dispersive interactions of R- and S-2-aminobutane with the π-system depends on the configuration of the solvent molecule. The result is a large, easily measurable difference of the spectral red-shifts of the homo- and heterochiral complexes ($\Delta\Delta\nu = +17$ cm$^{-1}$ for $E_R \cdot A_{R/S}$).[122]

The $CF_3$ group of $FE_R$ allows the establishment of intense NH•••F interactions with the selected amines which orient them away from to the aromatic ring. This reduces the enantioselectivity of $FE_R$ when compared with that of the $E_R$ where any intracomplex NH•••F bonding is obviously absent. No pronounced differences of the spectral red-shifts have been measured for the most stable conformers of the $[FE_R \cdot A_R]$ and $[FE_R \cdot A_S]$ complexes ($\Delta\Delta\nu$
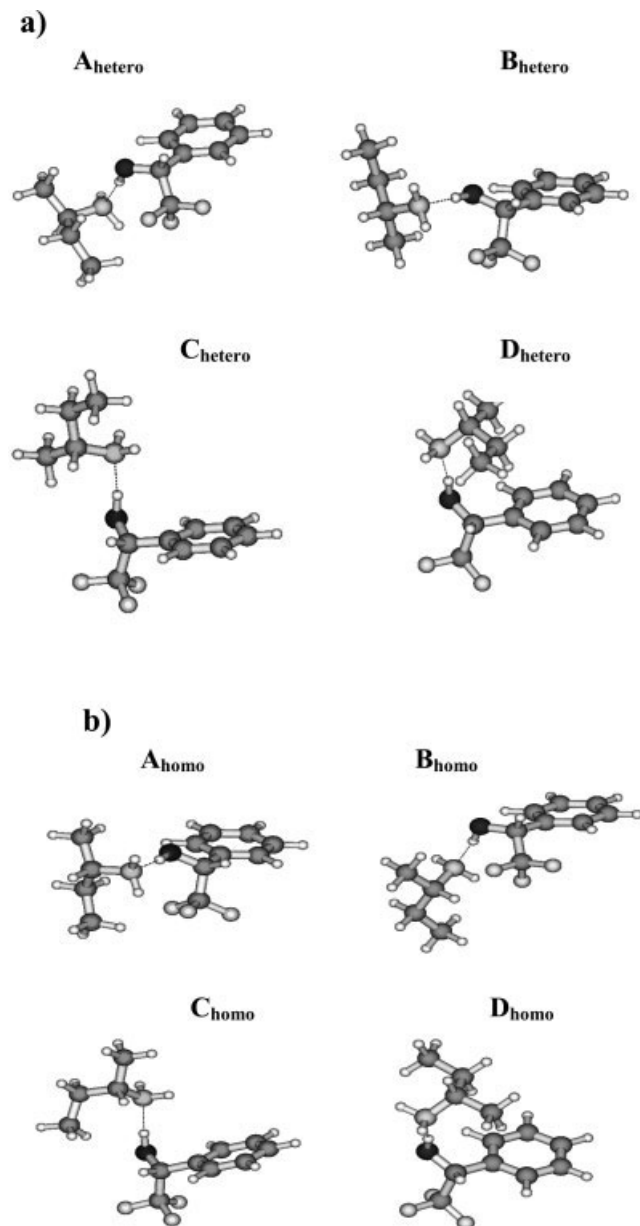
## a)



**A**hetero  **B**hetero

**C**hetero  **D**hetero

## b)

**A**homo  **B**homo

**C**homo  **D**homo

**Fig. 13.** Ab initio B3LYP/6-31G** calculated structures of the complex of **FE**$_R$ with (**a**) **A**$_R$ and (**b**) **A**$_S$.

= −2 cm$^{-1}$). Instead, $\Delta\Delta\nu$ values, approaching those of **E**$_R$•**A**$_{R/S}$, are measured for the D$_{homo}$/D$_{hetero}$ ($\Delta\Delta\nu$ = −13 cm$^{-1}$) and C$_{homo}$/C$_{hetero}$ ($\Delta\Delta\nu$ = +17 cm$^{-1}$) pairs of [**FE**$_R$•**A**$_{R/S}$]. This similarity is not fortuitous because the D$_{homo}$/C$_{homo}$ and D$_{hetero}$/C$_{hetero}$ pairs are the only among the [**FE**$_R$•**A**$_R$] and [**FE**$_R$•**A**$_S$] conformers wherein the amine moiety may somehow interact with the aromatic ring of the chromophore, much like in the [**E**$_R$•**A**$_{R/S}$] and [**P**$_R$•**A**$_{R/S}$] complexes.

### Furanose Rings Analogues: R- and S-3-Hydroxytetrahydrofuran

Because of their similarity to the furanose rings of nucleotides, the R-(−)- (**Th**$_R$) and S-(+)-3-hydroxytetrahy-

drofuran (**Th**$_S$) enantiomers can be considered as a prototypical building block of living matter. Like many other five-membered rings, **Th**$_R$ and **Th**$_S$ may assume in the isolated state several ring-puckering conformations.[120] In the most stable one, the hydrogen atom of the alcoholic function (henceforth denoted as O$^{al}$—H) points toward the ethereal oxygen atom (henceforth denoted as O$^{et}$), establishing a weak hydrogen bond interaction. DFT calculations indicate that the PA of **Th** at the O$^{et}$ center (PA = 861 kJ mol$^{-1}$) exceeds that at the O$^{al}$ one (PA = 831 kJ mol$^{-1}$) by about 30 kJ mol$^{-1}$. Therefore, the O$^{et}$ atom is the most basic center in **Th**. Because of the presence of two functional groups, **Th**$_R$ and **Th**$_S$ may give rise to several different possible structures when associated with other molecules.[124]

R-(+)-1-Phenyl-1-propanol (**P**$_R$) was chosen as the model chiral receptor for **Th**$_R$ and **Th**$_S$. We have often used this chromophore as a probe of the noncovalent interactions in diastereomeric complexes. **P**$_R$ is a floppy molecule, characterized by the presence of three low-energy conformational minima in the ground-state potential-energy surface (PES), which originates by rotation of the ethyl group around the C$_\alpha$-C$_\beta$ bond. The most stable *anti* conformer and at least one *gauche* rotamer have been identified in the electronic spectrum of the bare molecule.[115,125]

The intramolecular hydrogen bond, usually operative in bifunctional alcohols (solv) in the gas phase, can be either retained or disrupted and replaced by a more stabilizing intermolecular hydrogen bond network when solv is associated with a protic chromophore, like **P**$_R$. The hydrogen bond networks can be classified in three groups (Fig. 14): (1) where the chromophore acts as the H-donor to the most basic site of solv (:Y in Fig. 14). These structures exhibit also a weak O$^{al}$–H•••$\pi$ interaction between the alcoholic group of solv and the $\pi$ system of the chromophore (Y$^{add}$ in Fig. 14); (2) where the chromophore acts as the H-donor to the less basic *n*-type site of solv (O$^{al}$ in Fig. 14). These structures show an intramolecular O$^{al}$–H•••Y interaction between the functional groups of solv (O$^{add}$ in Fig. 14); and (3) where the **O**H group of the chromophore acts either as the H-donor to the most basic :Y site of solv and as the H-bond acceptor from its O$^{al}$–H alcoholic function (O$^{ins}$ in Fig. 14). All three structures have been recognized on the DFT calculated PES of both the heterochiral [**P**$_R$•**Th**$_S$] and the homochiral [**P**$_R$•**Th**$_R$] complexes (Fig. 15a). Structures **I**$_{homo}$ and **I**$_{hetero}$ present two intense intermolecular **O**—H•••O$^{et}$ and O$^{al}$—H•••**O** interactions. These structures are classified as "insertion" complexes, because the **O**H group of the chromophore is inserted into the intramolecular hydrogen bond of **Th**, and acts either as the H-donor to the most basic site of **Th** and as the H-bond acceptor from its O$^{al}$—H alcoholic function. Complexes **II**$_{homo}$ and **II**$_{hetero}$ are instead characterized by an intermolecular **O**—H•••O$^{al}$ hydrogen bond with the less basic site of Th. In these "addition-type" structures, the intramolecular O$^{al}$—H•••O$^{et}$ interaction between the functional groups of **Th** is somewhat maintained. Finally, structures **III**$_{homo}$ and **III**$_{hetero}$ exhibit an intermolecular **O**—H•••O$^{et}$ interaction with the most basic site of **Th** and a weaker O$^{al}$—H•••$\pi$ one between the alcoholic group of **Th** and the $\pi$ system of the chromophore. Analogous
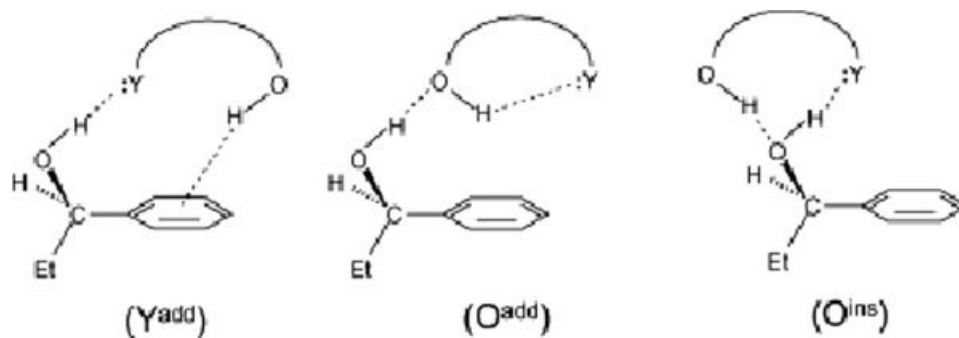
**Fig. 14.** Schematic representation of the most common structures for gas-phase complexes between (*R*)-(+)-1-phenyl-1-propanol (**P$_R$**) and bifunctional alcohols (:Y most basic center of the alcoholic solv).

structures were found for the [**P$_R$·Th$_{R/S}$**] clusters involving the *gauche* rotamers of the chromophore.[120]

Figures 16a and 16b show the 1cR2PI excitation spectrum of the homochiral [**P$_R$·Th$_R$**] and the heterochiral cluster [**P$_R$·Th$_S$**], respectively. These spectra are characterized by several bands red- (the α bands) or blue-shifted (the β and γ bands) relative to the $0_0^0$ electronic origin of

the most stable conformer of the **P$_R$** chromophore (Table 2). The magnitude of the relevant Δν values is related to the variation of bonding efficiency in the π and π* states and is found to decrease in passing from the heterochiral [**P$_R$·Th$_S$**] to the homochiral [**P$_R$·Th$_R$**] cluster.

Different 2c-R2PI appearance thresholds have been measured for the diastereomeric [**P$_R$·Th**]$^{•+}$ ions at their



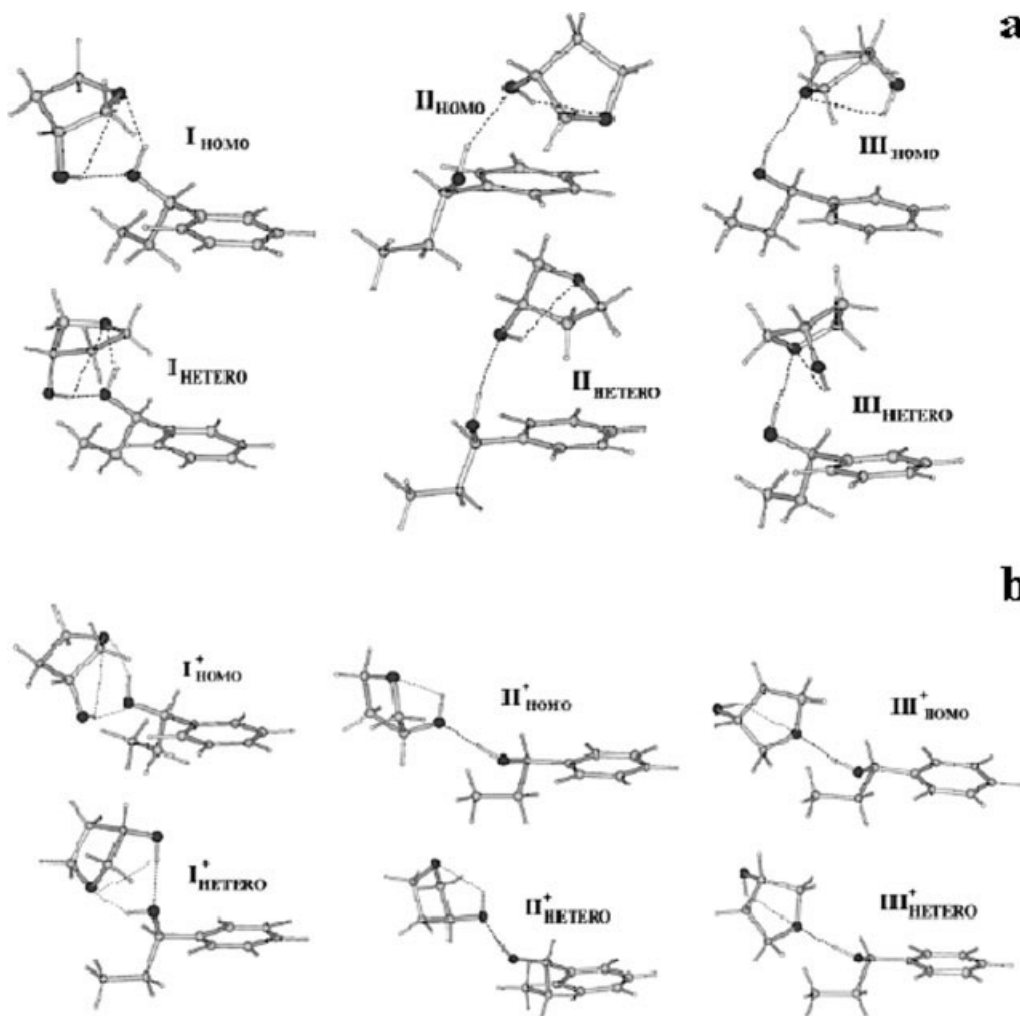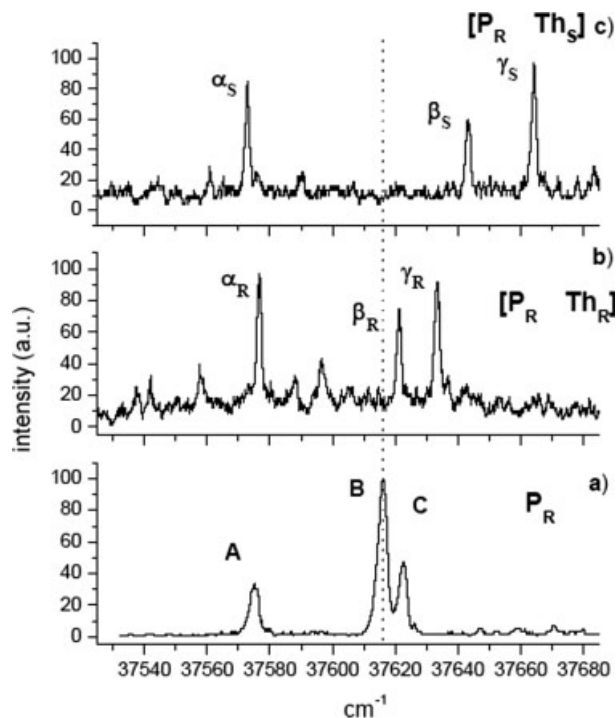**Fig. 15.** DFT-calculated [**P$_R$·Th**] and [**P$_R$·Th**]$^{•+}$ equilibrium isomeric structures: (**a**) neutral clusters (**b**) ionic structures.

**Fig. 16.** (**a**) 1cR2PI excitation spectra of (*R*)-(+)-1-phenyl-1-propanol (a) and its complexes with (**b**) (*R*)-(−)-3-hydroxytetrahydrofuran ([**P$_R$·Th$_R$**]) and (**c**) (*S*)-(+)-3-hydroxytetrahydrofuran ([**P$_R$·Th$_S$**]), obtained by monitoring the ion signal at the ethyl loss fragment mass (*m/z* 195). The dashed line refers to the $0_0^0$ transition for the more stable *anti* conformer of bare **P$_R$**.

relevant $\alpha - \gamma$ frequencies ($^{exp}IE_{(cluster)}$ in Table 3). The $C_\alpha$-$C_\beta$ fragmentation thresholds for the $\alpha$, $\beta$, and $\gamma$ bands ($^{exp}AE^{-Et}$ in Table 3) are different as well. This enables us to safely ascribe each of the $\alpha - \gamma$ (and $\alpha' - \gamma'$) bands to a different conformational isomer. The assignment of the $\alpha - \gamma$ bands to different isomeric forms was by no means an easy task. The formation of the adducts with the three **P$_R$** rotamers has been excluded by comparisons with the excitation spectra of the complexes of **P$_R$** with analogues monodentate solvents (ciclopentanol, tetrahydrofuran, and secondary alcohols).[120] Therefore, the $\alpha - \gamma$ bands of Figure 16 have been attributed to the three dominant isomeric forms **I**, **II**, and **III** reported in Figure 15a.

As pointed out in related articles,[126,127] the bathochromic shifts of the $0_0^0$ electronic $S_1 \leftarrow S_0$ origin, observed when **P$_R$** is complexed with an alcohol, is phenomenologically related to the increase of the electron density on the oxygen center of the chromophore by O—H···O hydrogen bonding with the O atom of the solvent. Similarly important are dispersive interactions between the aliphatic chain of the alcohol and the π-system of the chromophore, which are mainly responsible of the different spectral shifts observed when also the alcoholic solvent is chiral. Careful examination of the calculated structures (see Ref. 120) has led to the assignment reported in Table 2.

Some considerations have to be made about the relative intensity of the three $\alpha - \gamma$ bands. At first glance, one would predict the most intense band $\beta$ as corresponding to the most stable insertion complexes **II**. The different assignment of Table 2 is to be ascribed to the deformation energy (calculated to be 5 kJ mol$^{-1}$ for [**P$_R$·Th$_R$**] and 7 kJ mol$^{-1}$ for [**P$_R$·Th$_S$**]) required for inserting the **O**H group of the chromophore in the intramolecular hydrogen bond of the **Th**. Indeed the "insertion" form was never experimentally identified among the jet-cooled complexes of *R*- or *S*-2-naphthyl-1-ethanol with amino alcohols, presumably because of the large deformation energy (ca. 13 kJ mol$^{-1}$) accompanying insertion of the OH group of the chromophore into the strong intramolecular H-bond in amino alcohols.[120]

R2PI studies on **P$_R$**[6,8] and 1-phenyl-1-ethanol (**E$_R$**)[122] showed that, after photoionization, their clusters may fragment by homolytic $C_\alpha$-$C_\beta$ bond cleavage. The relevant energy barriers are much lower in the radical ionic states than in the neutral electronic states and the efficiency of the fragmentation is enhanced when a hydrogen-bond interaction is present between the chromophore and the solvent molecule. This low energy $C_\alpha$-$C_\beta$ bond dissociation was ascribed to an intersection between the potential energy surfaces of the lowest energy electronic states of the radical cations, which are perturbed by the interaction with a solvent molecule. The effects of microsolvation by water and chiral diols on the energetics and dynamics of photodissociation of $C_\alpha$-$C_\beta$ bond of **P$_R$**$^{•+}$ were analyzed by measuring their fragmentation thresholds.[8,128] It was demonstrated that the energy barrier for this process depends on the proton affinity of the partner and on its configuration.

A thorough examination of the effects of asymmetric microsolvation of **P$_R$** with chiral **Th$_R$** and **Th$_S$** on the energetics and dynamics of photo-dissociation of $C_\alpha$-$C_\beta$ bond in the **P$_R$** ionized chromophore is reported here. Table 3 reports the fragmentation thresholds ($^{exp}AE^{-Et}$) for the **I**–**III** isomers of [**P$_R$·Th$_S$**] and [**P$_R$·Th$_R$**] as measured in a two-color R2PI sequence with the first photon ($h\nu_1$) at resonance with the $0_0^0$ $S_1 \leftarrow S_0$ electronic transition of each $\alpha$,

**TABLE 2. R2PI absorption frequencies of [P$_R$·Th$_{R/S}$] isomers and band shifts of the electronic transition**

| Complex | Band | $\nu_1$ (cm$^{-1}$) | $\Delta\nu$ (cm$^{-1}$) | Structure assignment | Type of complex |
|---|---|---|---|---|---|
| [**P$_R$·Th$_S$**] | $\alpha_S$ | 37573 | −45 | **II$_{hetero}$** | O$^{al}$ addiction |
| | $\beta_S$ | 37643 | +25 | **I$_{hetero}$** | insertion |
| | $\gamma_S$ | 37664 | +46 | **III$_{hetero}$** | O$^{et}$ addiction |
| [**P$_R$·Th$_R$**] | $\alpha_R$ | 37576 | −42 | **II$_{homo}$** | O$^{al}$ addiction |
| | $\beta_R$ | 37622 | +4 | **I$_{homo}$** | insertion |
| | $\gamma_R$ | 37634 | +16 | **III$_{homo}$** | O$^{et}$ addiction |

**TABLE 3. Ethyl-loss fragmentation thresholds and activation energies for the ethyl radical loss from the [$P_R$•solv]•+ ions**

| Ionic species | Isomeric structure | Experimental $C_\alpha$-$C_\beta$ fragmentation threshold $^{exp}AE^{-Et}$ (cm$^{-1}$)[a] | Calculated ionization potential (see text) $^{exp/th}IP$ (cm$^{-1}$)[b] | Activation energies $E_{act}$ (cm$^{-1}$)[b,c] | Relative stability in the ionic state $^{th}\Delta E_+$ (cm$^{-1}$)[b] |
|---|---|---|---|---|---|
| [$P_R$•$Th_R$] | $I_{homo}(\beta_R)$ | 72,500 | 68,942 | 3558 | 819 |
| | $II_{homo}(\alpha_R)$ | 71,385 | 67,270 | 4115 | 0 (most stable) |
| | $III_{homo}(\gamma_R)$ | 72,185 | 68,507 | 3678 | 752 |
| [$P_R$•$Th_S$] | $I_{hetero}(\beta_S)$ | 72,435 | 68,499 | 3936 | 535 |
| | $II_{hetero}(\alpha_S)$ | 71,585 | 67,830 | 3755 | 392 |
| | $III_{hetero}(\gamma_S)$ | 71,960 | 68,331 | 3629 | 552 |

[a]Uncertainty level: ±100 cm$^{-1}$.
[b]Uncertainty level: ±140 cm$^{-1}$.
[c]$E_{act} = {}^{exp}AE^{-Et} - {}^{exp/th}IP_{(cluster)}$.

$\beta$, and $\gamma$ isomer (see also Fig. 17). The phenomenological fragmentation threshold $^{exp}AE^{-Et}$ refers to the process: [$P_R$•Th] + $h\nu_1$ → [$P_R$•Th]* + $h\nu_2$ → [($P_R$-$C_2H_5$)•Th]$^+$ + •$C_2H_5$. The products of this fragmentation reaction are the ethyl radical (•$C_2H_5$) and the solvated closed-shell cation [($P_R$-$C_2H_5$)•Th]$^+$.

The $^{exp}AE^{-Et}$ values of Table 3 span over a limited energy range from 71,585 to 72,435 cm$^{-1}$ for [$P_R$•$Th_S$] and from 71,385 to 72,500 cm$^{-1}$ for [$P_R$•$Th_R$]. Also, the energy range is even narrower when comparing the diastereomeric pairs $I_{hetero}$/$I_{homo}$, $II_{hetero}$/$II_{homo}$, and $III_{hetero}$/$III_{homo}$ pairs, the major $^{exp}AE^{-Et}$ difference being observed for the latter (225 cm$^{-1}$).

The activation energies $E_{act}$ for the reaction: [$P_R$•Th]•$^+$ → [($P_R$-$C_2H_5$) •Th]$^+$ + •$C_2H_5$, can be calculated from the difference between the phenomenological fragmentation threshold ($^{exp}AE^{-Et}$) and the ionization potential of the clusters. The ionization potential of the clusters were derived from experimental and theoretical data[120] and are also reported in Table 3.

As it can be seen from Table 3, the magnitude of $E_{act}$ depends upon the configuration of the solvent molecule as well as its specific H-bonded structure, whether $O^{al}$ addiction, $O^{et}$ addiction, or insertion. Moreover, the minimum energy required to cleave the $C_\alpha$-$C_\beta$ bond in the isolated $P_R$ has been measured to be 7470 cm$^{-1}$.[128] This means that H-bond interaction with the partner substantially alters the topology of the intersection region of the two ionic potential energy surfaces involved in the dissociation, resulting in much lower values of $E_{act}$ in H-bonded clus-
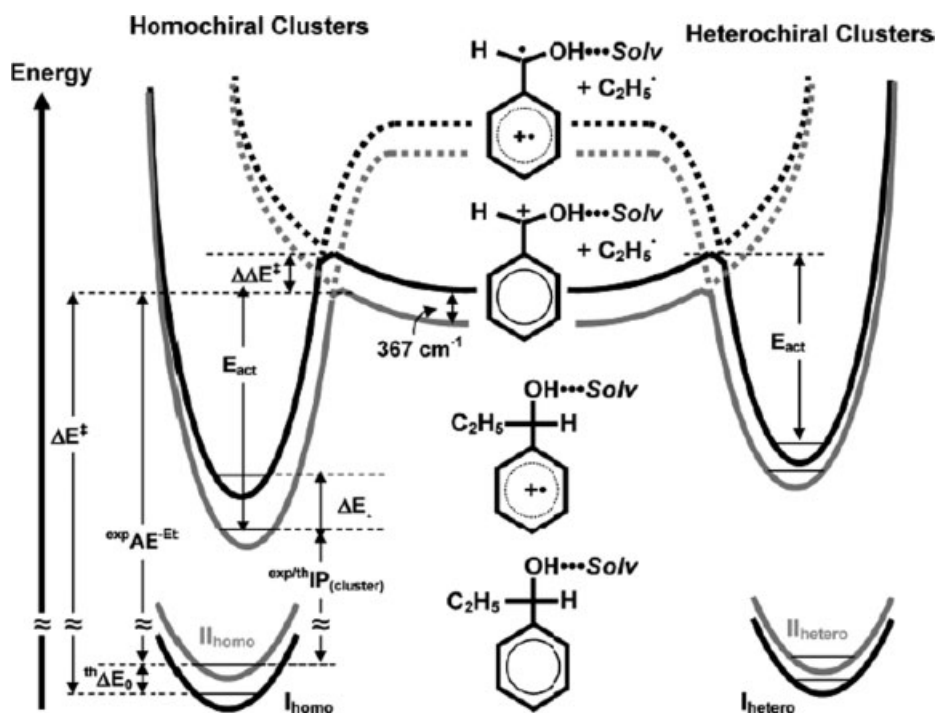


**Fig. 17.** Schematic representation of the potential energy curves for isomers **I** (black lines) and **II** (grey lines) of the homochiral [$P_R$•$Th_R$] complex (left) and the heterochiral [$P_R$•$Th_S$] complex (right). The curves relative to structures **III** are similar to those of **II** and are omitted for the sake of clarity. The potential wells and the dissociation limits refer to the species shown in the center of the figure.
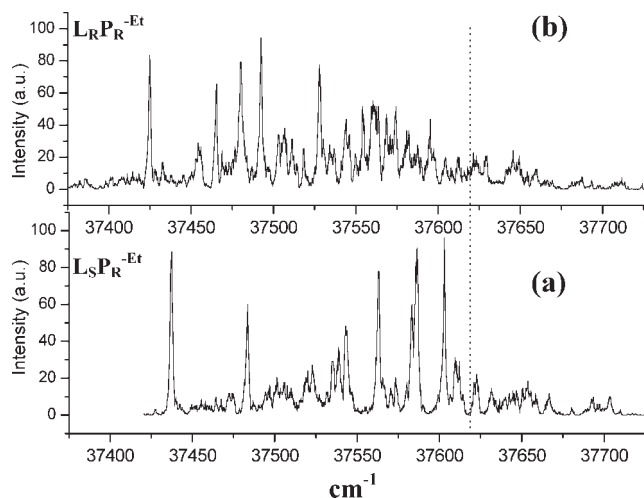
**Fig. 18.** 1cR2PI excitation spectra of the complexes of $P_R$ with $L_R$ (a) and $L_S$ (b). The origin of the frequency scale is relative to the $0_0^0$ transition for the most stable conformer of the $P_R$ chromophore at 37,618 cm$^{-1}$ and is marked as a dashed line.

ters. As previously found in other complexes,[8,128] hydrogen bond interaction activates the inductive and electrostatic forces which control the PES and the charge transfer process involved in the homolytic dissociation.

Table 3 gives also the DFT computed relative energies $^{th}\Delta E_+$ of the corresponding $[P_R \cdot Th]^{\bullet+}$ ion isomeric structures, i.e., the relative stability of the clusters in the ionic state (Figs. 15b and 17).

Comparison of the two sets of data, $^{th}\Delta E_+$ and $E_{act}$, in Table 3 confirms previous views about the existence of an inverse relationship between them.[8,128] For all $[P_R \cdot Th_R]^{\bullet+}$ isomers and for structures $I_{hetero}$ and $III_{hetero}$ of $[P_R \cdot Th_S]^{\bullet+}$, the greater the stability of the ionic adducts, the greater its fragmentation barrier $E_{act}$.[8,128] This means that the different total energy between the $O-H \cdots O^{et}$ bonded $[(P_R C_2 H_5) \cdot Th]^+$ fragment and the more stable $O-H \cdots O^{al}$ bonded one plays only a minor role in determining different activation energies, the major role being played by the much greater $\Delta E^+$ ion stability differences (Table 3).

The $E_{act}$ of the $II_{hetero}$ structure of $[P_R \cdot Th_S]^{\bullet+}$ does not follow the same trend. This can be attributed to the fact that, at variance with what is observed for the homochiral $[P_R \cdot Th_R]^{\bullet+}$ isomers, the $\Delta E^+$ differences for the heterochiral $[P_R \cdot Th_S]^{\bullet+}$ structures are much narrower. These findings would suggest that the different activation energies for the heterochiral $[P_R \cdot Th_S]^{\bullet+}$ structures are not only influenced by the stability of the relevant ionic adducts, but also by the stability difference between the solvated final products.

### Chiral Carboxylic Esters

Carboxylic compounds substituted at the α-position play a prominent role in a variety of important medical and pharmaceutical applications.[129,130] From the point of view of basic research, these compounds look very interesting and challenging owing to the α-substituent adjacent to the

carboxylic group which allows many possible intramolecular interactions in the isolated molecule and a variety of intermolecular interactions in its clusters with suitable acceptors. The practical importance of α-substituted carboxylic compounds in medical and pharmaceutical sciences is increased by the fact that most of these molecules are chiral. In view of the importance of these carboxylic compounds in life sciences, we undertook a detailed study on the complexes of $P_R$ with methyl lactates ($L_R$ and $L_S$), methyl 3-hydroxybutyrates ($H_R$ and $H_S$), and methyl 2-chloropropionates ($C_R$ and $C_S$), as model systems. The substitution of the COOH group by COOCH$_3$ restricts the number of possible hydrogen bond interactions and, therefore, makes the study much easier. These bifunctional molecules present intramolecular O–H···O=C hydrogen bonding in the isolated state and may exist in distinct conformations. As pointed out above, intramolecular interactions in bifunctional solv, such as $L_R$ and $L_S$, may be replaced by multiple intermolecular interactions in complexes with alcoholic chromophores, like $P_R$.

The 1cR2PI excitation spectra of the isomeric complexes of $P_R$ with the selected carboxylic esters are illustrated in Figures 18–20. The spectra were measured at the ion signal of the ethyl loss fragmentation product. Their spectral patterns are characterized by an ensemble of bands red- or blue-shifted relative to the $0_0^0$ electronic $S_1 \leftarrow S_0$ origin of the most populated *anti* conformer of the bare chromophore $P_R$ (at 37,618 cm$^{-1}$, marked in the Figures 18–20 with a broken line).

The spectral patterns of the homochiral $[L_R \cdot P_R]$ and heterochiral $[L_S \cdot P_R]$ complexes (Figs. 18a and 18b, respectively), are characterized by the presence of five intense bands all red-shifted relative to the band origin of the most stable isomer of the bare chromophore $P_R$. No blue-shifted signals were observed for these 1:1 complexes. Concerning the nature of these five signals, it is well established that association of $P_R$ with bidentate solv,
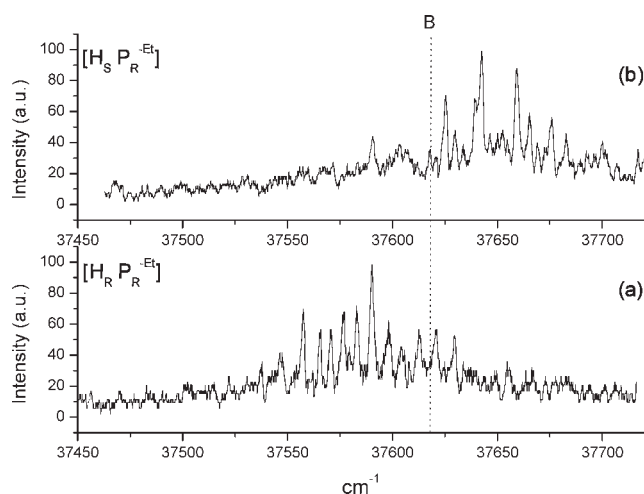


**Fig. 19.** 1cR2PI excitation spectra of the complexes between $P_R$ and $H_R$ (a) and $H_S$ (b). The origin of the frequency scale is relative to the $0_0^0$ transition for the most stable conformer of the $P_R$ chromophore at 37,618 cm$^{-1}$ and is marked as a dashed line.
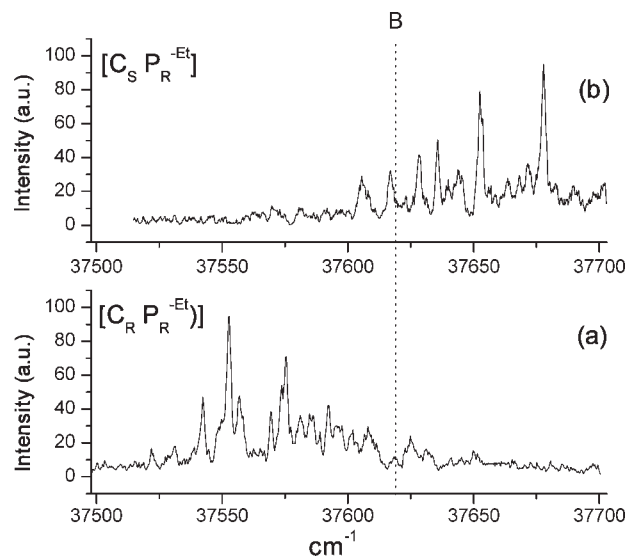
**Fig. 20.** 1cR2PI excitation spectra of the complexes between $\mathbf{P_R}$ and $\mathbf{C_R}$ (a) and $\mathbf{C_S}$ (b). The origin of the frequency scale is relative to the $0_0^0$ transition for the most stable conformer of the $\mathbf{P_R}$ chromophore at 37,618 cm$^{-1}$ and is marked as a dashed line.

like the selected esters, can markedly unbalance the relative population of the rotamers of the chromophore to the point that only one $\mathbf{P_R}$ conformer predominates.[120] This view is further confirmed by DFT-calculated structures of the most stable diastereomeric $[\mathbf{L_R \cdot P_R}]$ and $[\mathbf{L_S \cdot P_R}]$ isomers (Fig. 21). It can be observed that the number of stable $[\mathbf{L_R \cdot P_R}]$ and $[\mathbf{L_S \cdot P_R}]$ isomers coincides with the number of intense signals of Figure 18. Among the DFT computed structures, the (a) and (b) rotamers, like the (a') and (b') ones, are structurally analogous to the members of the insertion complexes family (Fig. 14) because the

**O**H group of the chromophore is inserted into the intramolecular hydrogen bond of **L**. Structures (c) and (c') can be considered as belonging to the O addiction class, where the chromophore acts as the H-donor to the less basic *n*-type site of **L** (O). These structures show an intramolecular CO•••H—**O** interaction between the functional groups of **L**. Structures (d), (d'), (e), and (e') may be included in the CO addiction category where the chromophore acts as the H-donor to the most basic site of **L**. These structures exhibit also an O–H•••$\pi$ interaction between the alcoholic group of solv and the $\pi$ system of the chromophore. Only a tentative structural assignment of the measured red shifted bands was possible. Presumably, the least red-shifted bands of Figure 18a pertain to structure (e) and that of Figure 18b to structure (e'), because both are characterized by the alcoholic OH bond pointing to the $\pi$ system of $\mathbf{P_R}$ at relatively short O–H•••$\pi$ equilibrium distances. In analogy with previous evidence on secondary alchools,[120,127] we tend to assign the most red-shifted bands to the O$^{add}$-like structures (c) and (c') (see Ref. 121).

The 1cR2PI spectra of $[\mathbf{H_R \cdot P_R}]$ and $[\mathbf{H_S \cdot P_R}]$ (Fig. 19) show some similarity with the 1cR2PI spectra of $[\mathbf{C_S \cdot P_R}]$ and $[\mathbf{C_R \cdot P_R}]$ complexes (Fig. 20). Both heterochiral $[\mathbf{H_S \cdot P_R}]$ and $[\mathbf{C_S \cdot P_R}]$ complexes are characterized by the presence of several bands, most of them blue-shifted relative to the band origin of the bare chromophore $\mathbf{P_R}$. In contrast, the spectral patterns of the homochiral $[\mathbf{H_R \cdot P_R}]$ and $[\mathbf{C_R \cdot P_R}]$ complexes show several red-shifted bands relative to the band origin of the bare chromophore $\mathbf{P_R}$. Again, the experimental spectral shifts of Figures 19 and 20 were rationalized in terms of the structural parameters of the specific diastereomeric clusters.

The counterbalancing effects of dispersive and polar interactions in the most stable O$_{add}$ structures of the homochiral $[\mathbf{H_R \cdot P_R}]$ complex (Fig. 22) induce a small red
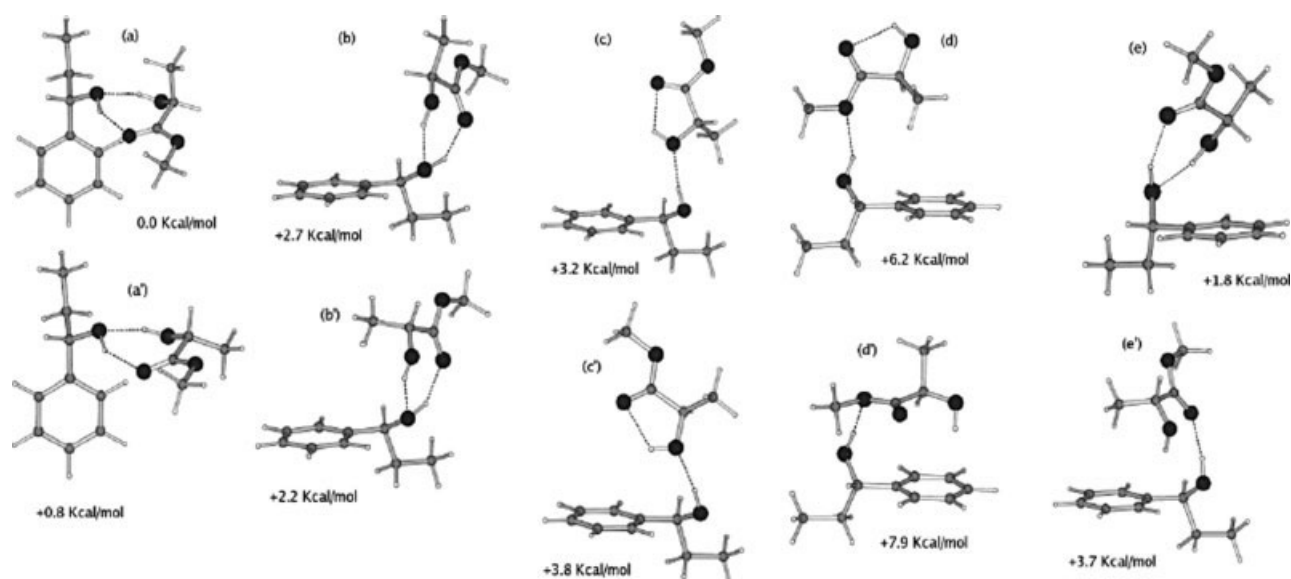


**Fig. 21.** B3LYP/6-31G-calculated structures of the diastereomeric $[\mathbf{L_{R/S} \cdot P_R}]$ clusters: (a–e) $[\mathbf{L_R \cdot P_R}]$; (a'–e') $[\mathbf{L_S \cdot P_R}]$.

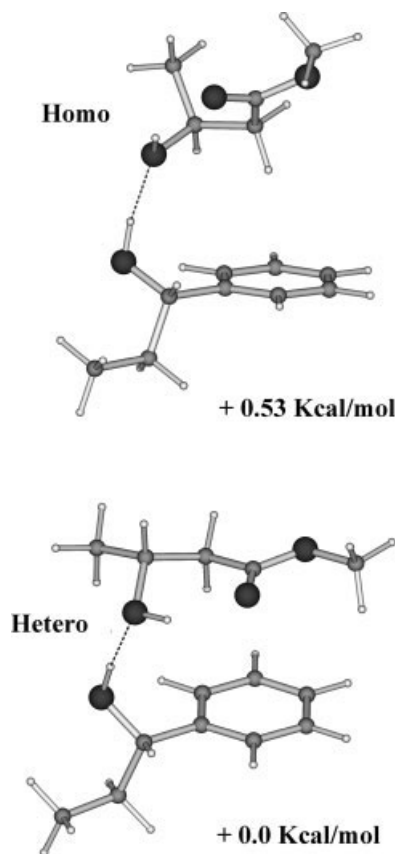**Fig. 22.** B3LYP/6-31G-calculated most stable structures of the diastereomeric $[H_{R/S} \cdot P_R]$ clusters: (a) $[H_R \cdot P_R]$; (a′) $[H_S \cdot P_R]$.

shift of its band origin. The same balance is missing in the heterochiral $[H_S \cdot P_R]$ complex (Fig. 22) because of the predominance of the polar over dispersive interactions which induces a small blue-shift of its band origin.

The geometrical structures and relative energies of the $[C_S \cdot P_R]$ and $[C_R \cdot P_R]$ adducts are shown in Figure 23. The red shifts in the $\pi \rightarrow \pi^*$ transition of the homochiral $[C_R \cdot P_R]$ cluster with respect to the bare $P_R$ could be accounted for by the dispersive interactions between the aromatic ring and the methyl group at C(3) of $C_R$. No similar red-shifts are observed with the heterochiral $[C_S \cdot P_R]$ cluster in conformity with the much weaker interactions between the aromatic ring of $P_R$ and the more removed methyl group at C(3). The blue-shifted bands of the heterochiral $[C_S \cdot P_R]$ cluster can be attributed to the polar interaction between the $\pi$-ring of the heterochiral $[C_S \cdot P_R]$ structure (c′) and the rather acidic ClCH hydrogen pointing toward it. The same interaction is prevented in the homochiral congener which in fact does not display any blue-shifted band relative to the bare chromophore.

### Neurotransmitters: (1S,2S)-N-Methylpseudoephedrine

Neurotransmitters are molecules which interpose between neurons (nerve cells), or between neurons and muscle cells. Detailed conformational studies on the simplest members of the class of neurotransmitters, as am-

phetamine, dopamine, noradrenaline, ephedrine, pseudoephedrine and others, has been accomplished[35,77–79],[97] by the analysis of the of the $S_1 \leftarrow S_0$ transition origins of their various conformers and by IR-R2PI determination of ground state frequencies. An important aspect of these studies concerns the conformational changes of the neurotransmitter molecule caused by monosolvation. No information however, is available regarding the van der Waals and hydrogen-bond interactions between a chiral solvent molecule and a neurotransmitter which, in effect, represents the basis of the receptor recognition of a chiral neurotransmitter molecule.

Our group was able to observe this aspect in a 1cR2PI-TOF spectroscopic study of a specific neurotrasmitter molecule, i.e., (1S,2S)-N-methylpseudoephedrine (**MPE**), involved in neuronal communication.[80] The effects of MPE asymmetric microsolvation by methyl R-lactate ($L_R$), methyl S-lactate ($L_S$), R-2-butanol ($B_R$), and S-2-butanol ($B_S$) have been investigated and compared with those of water (**W**) monosolvation. A common behavior of photo ionized ephedrine, pseudoephedrine, and their complexes, is that of undergoing extensive heterolitic $C_\alpha$-$C_\beta$ bond fragmentation to give the corresponding $[CH_3 CHNHCH_3]^+$ fragment ($m/z$ 58). Heterolitic $C_\alpha$-$C_\beta$ bond cleavage is even more extensive in **MPE** so that only the ion at $m/z$ 72 (corresponding to $[CH_3CHNH(CH_3)_2]^+$), is detected in the 1cR2PI-TOF mass spectrum (eq. 6).

$$\mathbf{MPE}^+ \rightarrow [CH_3CHN(CH_3)_2]^+ + PhCHOH\cdot \qquad (6)$$
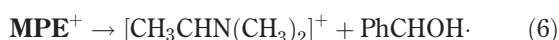
This behavior is favored by the presence of the second methyl group at the N center, resulting in an extra-stabilization of the positive charge of the fragment. Another major factor determining the almost complete $\mathbf{MPE}^{\bullet+}$ fragmentation is the large excess of energy ($\Delta E = E_{2h\nu} - IP \approx 1.8$ eV), imparted to the molecule by absorption of two photon during the 1cR2PI process ($E_{2h\nu} = 9.3$ eV). This excess energy is probably enough to overcome the barrier to fragmentation, if actually present. Important geometrical changes occur in the **MPE** molecule upon ionization. Frank-Condon factors leave the molecular cation in highly excited vibrational states leading to rapid fragmentation.

Also the 1cR2PI-TOF mass spectra of the diastereomeric $[\mathbf{MPE \cdot L_{R/S}}]$ complexes are characterized by their complete $C_\alpha$-$C_\beta$ fragmentation, accompanied by the loss of the $\mathbf{L_{R/S}}$ molecule. Their 1cR2PI-TOF absorption spectra, taken at $m/z$ 72 $[CH_3CHNH(CH_3)_2]^+$, were superimposed to that of the **MPE** molecule (Figs. 24a and 24b). Relative to the spectral features of **MPE**,[80] the spectral patterns of the diastereomeric $[\mathbf{MPE \cdot L_{R/S}}]$ complexes are characterized by addicional red-shifted bands (marked with asterisks in Fig. 24). The heterochiral complex exhibits only a single red-shifted peak ($\Delta \nu = -158$ cm$^{-1}$; Fig. 24a), whereas the homochiral one display two red-shifted bands ($\Delta \nu = -174$ and $-144$ cm$^{-1}$; Fig. 24b).

Seven ab initio HF/6-31G-optimized structures have been identified for each of the two diastereomeric $[\mathbf{MPE \cdot L_{R/S}}]$ forms with energy differences not exceeding 10 kcal mol$^{-1}$ (Fig. 25). As expected, a number of possible
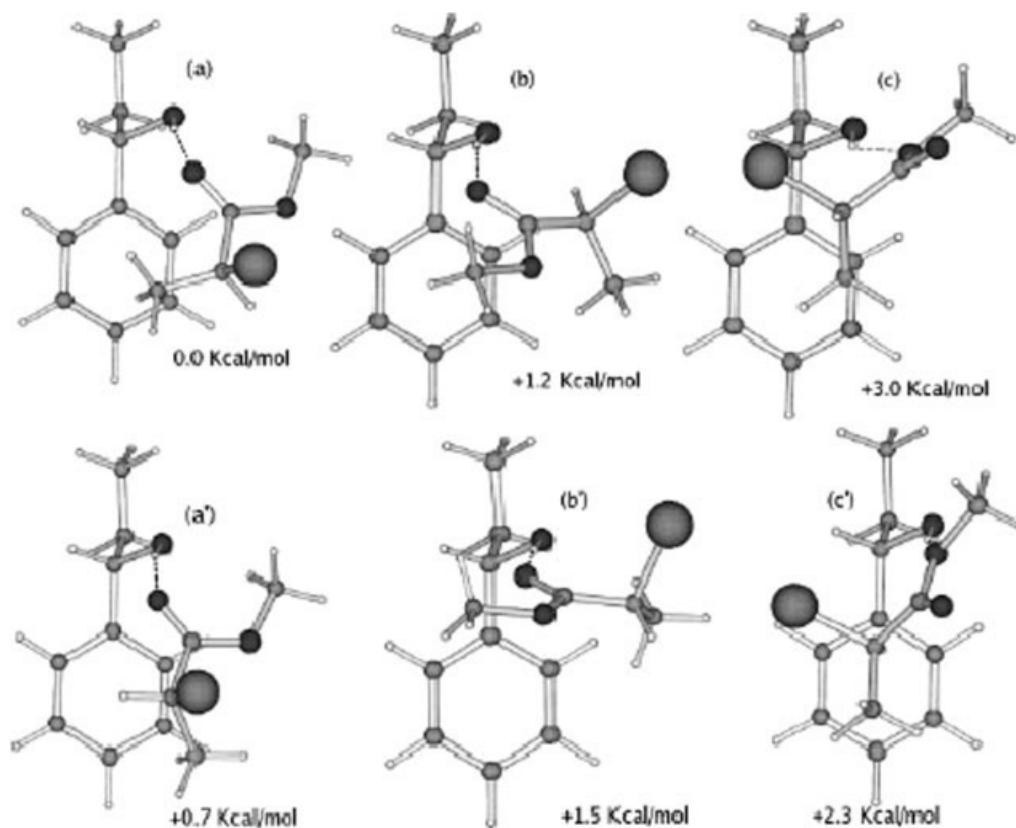
**Fig. 23.** B3LYP/6-31G-calculated structures of the diastereomeric $[C_{R/S} \cdot P_R]$ clusters: **(a–c)** $[C_R \cdot P_R]$; **(a′–c′)** $[C_S \cdot P_R]$.

hydrogen bonded structures are accessible because of the presence of several functionalities in both the chromophore and the solvent molecule. Inspection of the figure reveals that there is a close correspondence between the structure and the energy of the most stable homo- and the heterochiral adducts. In fact, the above structures have almost the same relative energies and geometries except for the interchange in the position of a methyl group with an hydrogen atom. The two red-shifted bands of the homochiral adduct have been attributed to the most stable degenerate A and B rotamers (Fig. 25). Analogously, the single red-shifted signal of the heterochiral complex is associated with the most stable A conformer. The slightly less stable structure B may not be sufficiently abundant at the low temperatures typical of supersonically expanded beams to produce a detectable signal.

Figure 26 reports the 1cR2PI mass spectrum of the clusters of **MPE** with the *s*-enantiomer of 2-butanol ($B_S$). At variance with what found for the $[\text{MPE} \cdot L_{R/S}]$ adducts, small amounts of both the desolvated $[\text{MPE}]^+$ and solvated fragments products $[CH_3CHN(CH_3)_2 \cdot B_S]^+$ were detected in the 1cR2PI-TOF mass spectra of $[\text{MPE} \cdot B_S]$. Very minor quantities of the intact $[\text{MPE} \cdot B_S]^+$ complex are detected as well. In this case, the low intensity of the peaks does not allow an accurate analysis of the 1cR2PI absorption spectra. Analogously, desolvated $[\text{MPE}]^+$ and solvated fragments products $[CH_3CHN(CH_3)_2 \cdot W]^+$ were identified in the 1cR2PI-TOF mass spectra of $[\text{MPE} \cdot W]$. It
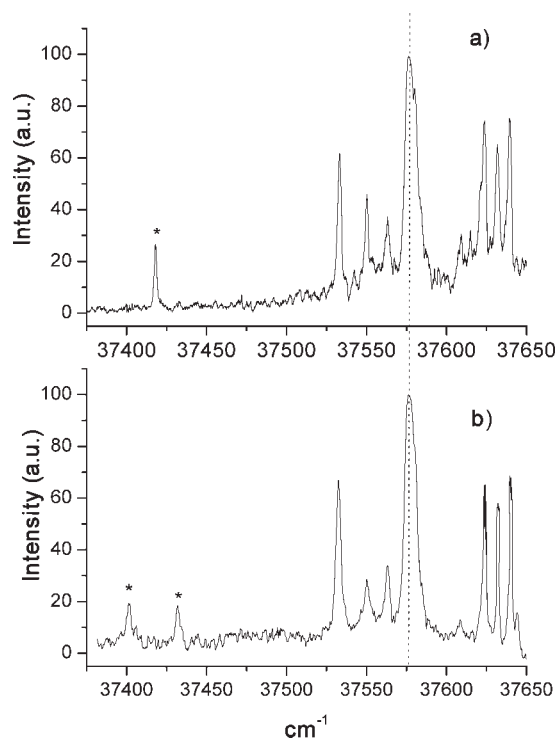


**Fig. 24.** 1cR2PI absorption spectrum of the MPE complex with methyl $(R)$-$(+)$-lactate $L_R$ (a) and methyl $(S)$-$(-)$-lactate $L_S$ (b) obtained by monitoring the fragment ion signals at $m/z$ 72.

was also established that these products originate from a common precursor, i.e., the [**MPE·W**]$^+$ complex.[80] One possible explanation for the minor fragmentations in [**MPE·B$_S$**]$^+$ and [**MPE·W**]$^+$ could be an appreciable increase of the ionization energy of **MPE** by solvation with **B$_S$** and **W**. Calculation of the IE of the more stable [**MPE·W**] structure[80] showed indeed an appreciable increase of its ionization potential with respect to that of the bare molecule.

## SUMMARY AND FUTURE DEVELOPMENTS

The main objective of this review article was to summarize the most recent applications of the R2PI technique in studies of tailor-made complexes containing chiral molecules of biological or pharmaceutical interest. The R2PI/TOF technique has proven to be a powerful tool for both the characterization of neutral solvated asymmetric structures and the investigation of enantiospecificic chemical reactivity in ion complexes. Some of the salient results are outlined below.
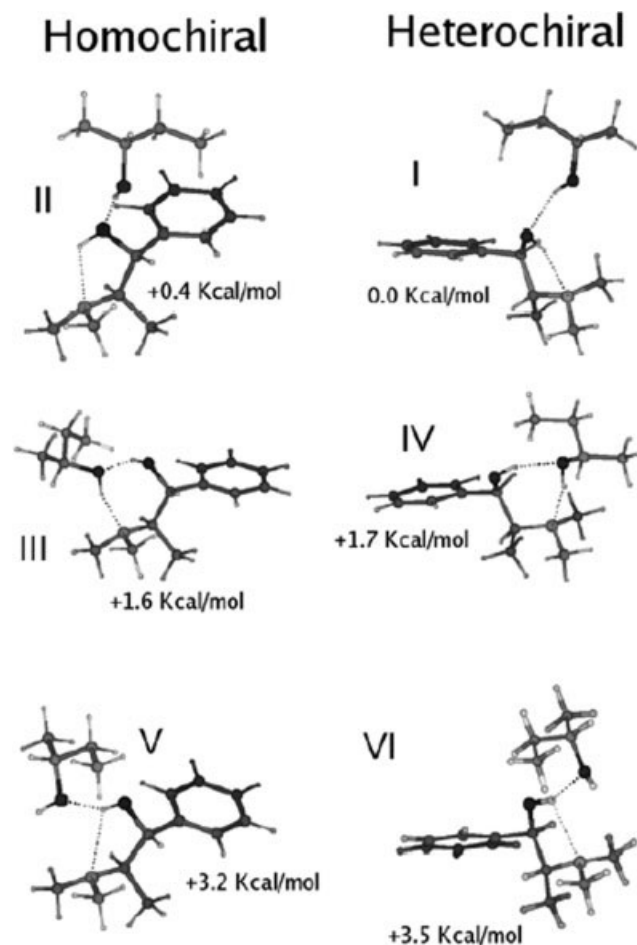


**Fig. 25.** Ab initio HF/6-31G most stable structures and predicted energies for the homochiral [**MPE·L$_S$**] and heterochiral [**MPE·L$_R$**] complexes.
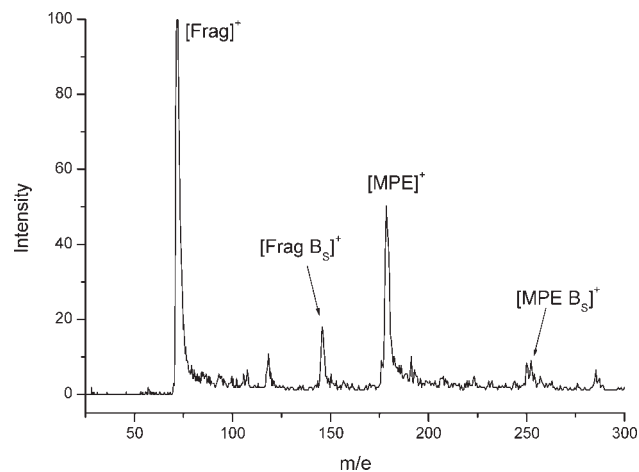
**Fig. 26.** 1cR2PI mass spectrum of the **MPE**/(*S*)-2-butanol mixture. The spectrum is measured at $\nu = 37{,}560$ cm$^{-1}$.

Detailed inspection of the experimental and theoretical results obtained for **E$_R$** and **FE$_R$** and their adducts with water and *R*- and *S*-2-ammminobutane enabled the observation of the effect of fluorine substitution in the molecular recognition and chiral recognition processes. It was found that the magnitude of dispersive interaction with the π-system is mainly responsible for different spectral enantioselectivity measured for diastereomeric complexes.

The CHOHCF$_3$ dissymmetric substituent on the aromatic ring of **FE$_R$** can induce an appreciable asymmetry in the π−electron density in both the ground and excited states, which is differently perturbed by interaction with Ar atoms.

The R2PI spectra measured for diastereomeric complexes containing fluoroaromatics, furanose rings analogues, esters, and neurotransmitters provide a viable means for spectroscopically discriminating enantiomers. Different conformational adjustment of the complexes is evident by the sign and the magnitude of the spectral shifts of the electronic transitions. These latter depend upon the configuration of the particular solvent molecule as well as on its specific H-bond interaction centers. The same factors play a major role in determining the magnitude of the activation barriers for the loss of an ethyl radical from [**P$_R$**·solv ] diastereomeric complex ions.

The concepts and methods developed during the last few years of intense work on relatively simple diastereomeric systems in the gas phase have paved the way to the study of more complicated biomolecular chiral systems. Furthermore, some experimental methodologies directly related to R2PI spectroscopy can be utilized in the near future for more advanced investigation of chiral discrimination in gas phase. Stimulated emission pumping spectroscopy is an interesting technique that provides insights into isomerization pathways.[131] High resolution vibrational structure of chiral ions could be obtained by Zero Electron Kinetic Energy (ZEKE) spectroscopy[29,30,109–111] and Mass-Analyzed Threshold Ionization (MATI) spectroscopy[132] which combine R2PI with sophisticated electronic detection.

Chiral discrimination could be investigated at subpico-second timescales[133–135] for chiral molecule/receptor pairs characterized by an ultrafast decay of the excited state. Time resolved experiments can follow ultrafast dynamics in real time, and therefore can provide more direct information about the mechanistic detail of excited-state and ion chemical reactions.

### LITERATURE CITED

1. Nir E, Kleinermanns K, De Vries MS. Pairing of isolated nucleic-acid bases in the absence of the DNA backbone. Nature 2000;408:949–951.

2. De Vries MS, Hobza P. Gas-phase spectroscopy of biomolecular building blocks. Annu Rev Phys Chem 2007;58:585–612.

3. Simons JP, Çarçabal P, Davis BG, Gamblin DP, Hünig I, Jockusch RA, Kroemer RT, Marzluff EM, Snoek LC. Sugars in the gas phase: spectroscopy, conformation, hydration, co-operativity and selectivity. Int Rev Phys Chem 2005;24:489–532.

4. Scoles G. Atomic and molecular beam methods, Vol. 1–2. New York: Oxford University Press; 1988.

5. Al-Rabaa AR, Breheret E, Lahmani F, Zehnacker A. Enantiodifferentiation in jet-cooled van der Waals complexes of chiral molecules. Chem Phys Lett 1995;237:480–484.

6. Piccirillo S, Bosman C, Toja D, Giardini A, Pierini M, Troiani A, Speranza M. Gas-phase enantiodifferentiation of chiral molecules. Chiral recognition of 1-phenyl-1-propanol/2-butanol cluster by resonance enhanced multiphoton ionization spectroscopy. Angew Chem Int Ed Engl 1997;36:1729–1731.

7. Latini A, Toja D, Giardini Guidoni A, Palleschi A, Piccirillo S, Speranza M. Energetics of molecular complexes in a supersonic beam: a novel spectroscopic tool for enantiomeric discrimination. Angew Chem Int Ed Engl 1999;38:815–817.

8. Catone D, Giardini Guidoni A, Paladini A, Piccirillo S, Rondino F, Satta M, Scuderi D, Speranza M. Homolytic C-C bond cleavage in a chiral alkylarene radical cation: effects of asymmetric microsolvation. Angew Chem Int Ed 2004;43:1868–1871.

9. Le Barbu K, Zehnacker A, Lahmani F, Mons M, Piuzzi F, Dimicoli I. Spectroscopic studies of enantiomeric discrimination in jet-cooled chiral complexes. Chirality 2001;13:715–721.

10. Wiley WC, McLaren IH. Time-of-flight mass spectrometer with improved resolution. Rev Sci Instrum 1955;26:1150–1157.

11. Neusser HJ, Krause H. Binding energy and structure of van der Waals complexes of benzene. Chem Rev 1994;94:1829–1843.

12. Helm RM, Vogel HP, Neusser HJJ. Rotational analysis and tunnel splittings of the intermolecular vibrations of the phenol–water complex by high resolution UV spectroscopy. Chem Phys 1998;108:4496–4504.

13. Pratt DW. High resolution spectroscopy in the gas phase: even large molecules have well-defined shapes. Annu Rev Phys Chem 1998;49:481–530.

14. Letokhov VS. On difference of energy levels of left and right molecules due to weak interactions. Phys Lett A 1975;53:275–276.

15. Quack M. How important is parity violation for molecular and biomolecular chirality? Angew Chem Int Ed Engl 2002;41:4618–4630.

16. Quack M, Stohner J, Willeke M. High-resolution spectroscopic studies and theory of parity violation in chiral molecules. Annu Rev Phys Chem 2008;59:741–769.

17. Brutschy B. Reactions in molecular clusters following photoionization. J Phys Chem 1990;94:8637–8647.

18. Piccirillo S, Coreno M, Bosman C, Giardini-Guidoni A, Mele A, Palleschi A. Resonant two-photon ionization of van der Waals adducts of 4-fluorostyrene with monomethylamine and monoethylamine: intracluster chemical reactions. Chem Phys Lett 1995;247:577–583.

19. Speranza M, Satta M, Piccirillo S, Rondino F, Paladini A, Giardini A, Filippi A, Catone D. Chiral recognition by mass-resolved laser spectroscopy. Mass Spectrom Rev 2005;24:588–610.

20. Lipert RJ, Colson SD. Persistent spectral hole burning of molecular clusters in a supersonic jet. J Phys Chem 1989;93:3894–3896.

21. Scherzer W, Selzle HL, Schlag EW. Identification of spectra of mixed structural isomers via mass selective hole-burning in the gas phase. Chem Phys Lett 1992;195:11–15.

22. Di Palma T, Latini A, Satta M, Varvesi M, Giardini A. Pulsed laser reactive ablation of Al in an ammonia atmosphere: photoionization thresholds and structures of Al–$NH_3$ clusters. Chem Phys Lett 1998;284:184–190.

23. Walters EA, Grover JR, White MG, Hui ET. On the structure and thermochemistry of the van der Waals molecule benzene-hydrogen chloride complex $C_6H_6 \cdot HCl$ and its photoion $(C_6H_6 \cdot HCl)^+$. J Phys Chem 1985;89:3814–3818.

24. Courty A, Mons M, Dimicoli N, Piuzzi F, Gaigeot MP, Brenner V, De Pujo P, Millie P. Quantum effects in the threshold photoionization and energetics of the benzene-$H_2O$ and benzene-$D_2O$ complexes: experiment and simulation. J Phys Chem A 1998;102:6590–6600.

25. Mons M, Piuzzi F, Dimicoli I, Zehnacker A, Lahmani F. Binding energy of hydrogen-bonded complexes of the chiral 1-phenylethanol molecule by 2C-R2PI: comparison between diastereoisomeric complexes with butan-2-ol and the singly hydrated complex. Phys Chem Chem Phys 2000;2:5065–5070.

26. Jortner J. Level structure and dynamics of clusters. Ber Bunsenges Phys Chem 1984;88:188.

27. Maerk TD, Castleman AW Jr. Experimental studies on cluster ions. Adv At Mol Phys 1984;20:65.

28. Gonohe N, Abe H, Mikami N, Ito M. Two-color photoionlzation of van der Waals complexes of fluorobenzene and hydrogen-bonded complexes of phenol in supersonic jets. J Phys Chem 1985;89:3642–3648.

29. Muller-Dethlefs K, Dopfer O, Wright TG. ZEKE spectroscopy of complexes and clusters. Chem Rev 1994;94:1845–1871.

30. Dessent CEH, Muller-Dethlefs K. Hydrogen-bonding and van der Waals complexes studied by ZEKE and REMPI spectroscopy. Chem Rev 2000;100:3999–4021.

31. Douin S, Piccirillo S, Bréchignac P. Solvation of charge in aromatic/noble gas Van der Waals clusters. Chem Phys Lett 1997;273:389–396.

32. Dao PD, Morgan S, Castelman AW. Two-color resonance enhanced multiphoton ionization of Van der Waals molecules: studies of spectroscopy shifts and ionization thresholds of paraxylene clustered with argon. Chem Phys Lett 1985;113:219–224.

33. Fuke K, Yoshiuchi H, Kaya K, Achiba Y, Sato K, Kimura K. Multi-photon ionization photoelectron spectroscopy and two-color multi-photon ionization threshold spectroscopy on the hydrogen bonded phenol and 7-azaindole in a supersonic jet. Chem Phys Lett 1984;108:179–184.

34. Satta M, Latini A, Piccirillo S, Di Palma TM, Scuderi D, Speranza M, Giardini A. Energetics of mono-hydrated chiral R(+) 1-phenyl-1-propanol: supersonic beam experiments and density functional calculations. Chem Phys Lett 2000;316:94–100.

35. Yao J, Im HS, Foltin M, Bernstein ER. Spectroscopy of neurotransmitters and their clusters: phenethylamine and amphetamine solvation by nonpolar, polar, and hydrogen-bonding solvents. J Phys Chem A 2000;104:6197–6211.

36. Page RH, Shen YR, Lee YT. Local modes of benzene and benzene dimer, studied by infrared–ultraviolet double resonance in a supersonic beam. J Chem Phys 1988;88:4621–4636.

37. Page RH, Shen YR, Lee YT. Infrared–ultraviolet double resonance studies of benzene molecules in a supersonic beam. J Chem Phys 1988;88:5362–5376.

38. Riehn C, Lahmann C, Wassermann B, Brutschy B. IR depletion spectroscopy. A method for characterizing a microsolvation environment. Chem Phys Lett 1992;197:443–450.

39. Joost M, Bakker JM, Compagnon I, Meijer G, Von Helden G, Kabela M, Hobzac P, De Vries M. The mid-IR absorption spectrum of gas-phase clusters of the nucleobases guanine and cytosine. Phys Chem Chem Phys 2004;6:2810–2815.

40. Mons M, Robertson EG, Snoek LC, Simons JP. Conformations of 2-phenyl ethanol and its singly hydrated complexes: UV-UV and IR-UV ion-dip spectroscopy. Chem Phys Lett 1999;310:423–432.

41. Borho N, Suhm MA. Glycidol dimer: anatomy of a molecular handshake. Phys Chem Chem Phys 2002;4:2721–2732.

42. Farník M, Weimann M, Steinbach C, Buck U, Borho N, Adler TB, Suhm MA. Size-selected methyl lactate clusters: fragmentation and spectroscopic fingerprints of chiral recognition. Phys Chem Chem Phys 2006;8:1148–1158.

43. King AK, Howard BJ. A microwave study of the hetero-chiral dimer of butan-2-ol. Chem Phys Lett 2001;348:343–349.

44. Su Z, Borho N, Xu Y. Chiral self-recognition: direct spectroscopic detection of the homochiral and heterochiral dimers of propylene oxide in the gas phase. J Am Chem Soc 2006;128:17126–17131.

45. Ritchie B. Theory of the angular distribution of photoelectrons ejected from optically active molecules and molecular negative ions. Phys Rev A 1976;13:1411–1415.

46. Bowering N, Lischke T, Schmidtke B, Muller N, Khalil T, Heinzmann U. Asymmetry in photoelectron emission from chiral molecules induced by circularly polarized light. Phys Rev Lett 2001;86:1187–1190.

47. Garcia GA, Nahon L, Lebech M, Houver JC, Dowek D, Powis I. Circular dichroism in the photoelectron angular distribution from randomly oriented enantiomers of camphor. J Chem Phys 2003;119:8781–8784.

48. Turchini S, Zema N, Contini G, Alberti G, Alagia M, Stranges S, Fronzoni G, Stener M, Decleva P, Prosperi T. Circular dichroism in photoelectron spectroscopy of free chiral molecules: experiment and theory on methyl-oxirane. Phys Rev A 2004;70:14502/1–14502/4.

49. Lische T, Böwering N, Schmidtke B, Müller N, Khalil T, Heinzmann U. Circular dichroism in valence photoelectron spectroscopy of free unoriented chiral molecules: camphor and bromocamphor. Phys Rev A 2004;70:22507/1–22507/12.

50. Giardini A, Catone D, Stranges S, Satta M, Sacconi M, Piccirillo S, Turchini S, Zema N, Contini G, Prosperi T, Decleva P, Di Tommaso D, Fronzoni G, Stener M, Filippo A, Speranza M. Angle-resolved photoelectron spectroscopy of randomly oriented 3-hydroxytetrahydrofuran enantiomers. ChemPhysChem 2005;6:1164–1168.

51. Desfrancois C. Determination of electron binding energies of ground-state dipole-bound molecular anions. Phys Rev A 1995;51:3667–3675.

52. Zhou YU, Oostenbrink C, Jongejan A, Van Gunsteren WF, Hagen WR, De Leeuw SW, Jongejan JA. Computational study of ground-state chiral induction in small peptides: comparison of the relative stability of selected amino acid dimers and oligomers in homochiral and heterochiral combinations. J Comput Chem 2006;27:857–867.

53. Rekharsky MV, Inoue Y. Complexation and chiral recognition thermodynamics of 6-amino-6-deoxyB-cyclodextrin with anionic, cationic, and neutral chiral guests: counterbalance between van der Waals and Coulombic interactions. J Am Chem Soc 2002;124:813–826.

54. Bea I, Jaime C, Kollman P. Molecular recognition by β-cyclodextrin derivatives: molecular dynamics, free-energy perturbation and molecular mechanics/Poisson-Boltzmann surface area goals and problems. Theor Chem Acc 2002;108:286–292.

55. Zhou Y, Oostenbrink C, Van Gunsteren WF, Hagen WR, De Leeuw SW, Jongejan JA. Relative stability of homochiral and heterochiral dialanine peptides. Effects of perturbation pathways and force-field parameters on free energy calculations. Mol Phys 2005;103:1961–1969.

56. Hayes JM, Stein M, Weiser J. Accurate calculations of ligand binding free energies: chiral separation with enantioselective receptors. J Phys Chem A 2004;108:3572–3580.

57. Mori T, Inoue Y, Grimme S. Time dependent density functional theory calculations for electronic circular dichroism spectra and optical rotations of conformationally flexible chiral donor–acceptor dyad. J Org Chem 2006;71:9797–9806.

58. Thirumoorthy K, Nandi N. Comparison of the intermolecular energy surfaces of amino acids: orientation-dependent chiral discrimination. J Phys Chem B 2006;110:8840–8849.

59. Ju X-H, Xie L-J, Hua W-T, Xiao H-M. Intermolecular interaction and thermodynamic properties of N-methylacetamide and hydroxyacetonitrile dimers. J Phys Org Chem 2004;17:113–117.

60. Alkorta I, Elguero J. Self-discrimination of enantiomers in hydrogen-bonded dimers. J Am Chem Soc 2002;124:1488–1493.

61. Portmann S, Inauen A, Lüthi HP, Leutwyler S. Chiral discrimination in hydrogen-bonded complexes. J Chem Phys 2000;113:9577–9585.

62. Le Barbu-Debus K, Lahmani F, Zehnacker-Rentien A, Guchhait N, Panja SS, Chakraborty T. Fluorescence spectroscopy of jet-cooled chiral (±)-indan-1-ol and its cluster with (±)-methyl- and ethyl-lactate. J Chem Phys 2006;125:174305/1–174305/8.

63. Satta M, Sanna N, Giardini A, Speranza M. Microsolvation effects on the $\pi^{\star} \leftarrow \pi$ electronic transitions in simple aromatic chromophores: the role of the Slater-type Gaussian orbitals in the complete active space self-consistent field approach. J Chem Phys 2006;125:094101/1–094101/8.

64. Bernhardsson A, Forsberg N, Malmqvist P, Ross BO. A theoretical study of the $1B_{2u}$ and $1B_{1u}$ vibronic bands in benzene. J Chem Phys 1999;112:2798.

65. Sobolewski A, Domcke W. Ab initio investigations on the photophysics of indole. Chem Phys Lett 1999;315:293–298.

66. Foggi P, Neuwahl FVR, Moroni L, Salvi PR. $S_1 \rightarrow S_n$ and $S_2 \rightarrow S_n$ absorption of azulene: femtosecond transient spectra and excited state calculations. J Phys Chem A 2003;107:1689–1696.

67. Grimme S, Izgorodina EI. Calculation of 0–0 excitation energies of organic molecules by CIS(D) quantum chemical methods. Chem Phys 2004;305:223–230.

68. Sobolewski AL, Adamowicz L. Theoretical investigations of the proton transfer reaction in the hydrogen-bonded complex of 2-pyrimidinone with water. J Phys Chem 1995;99:14277–14284.

69. Kim KS, Tarakeshwar P, Lee JY. Molecular Clusters of π-Systems: theoretical studies of structures, spectra, and origin of interaction energies. Chem Rev 2000;100:4145–4186.

70. Cai ZL, Reimers JR. The first singlet (n,π*) and (π,π*) excited states of the hydrogen-bonded complex between water and pyridine. J Phys Chem A 2002;106:8769–8778.

71. Ullrich S, Muller-Dethlefs K. A REMPI and ZEKE spectroscopic study of trans-acetanilide·H$_2$O and comparison to ab initio CASSCF calculations. J Phys Chem A 2002;106:9188–9195.

72. Ross BO, Anderson K, Fulscher MP, Malmquist P, Serrano-Andreas L. Multiconfigurational perturbation theory: applications in electronic spectroscopy. Adv Chem Phys 1996;93:219.

73. Li Y, Francisco JS. State-averaged CASSCF and MRCI studies on the ground and low-lying singlet excited states of methylacetylene. Spectrochim Acta A 1999;55:477–485.

74. Rubner O, Engel V, Hachey MR, Daniel C. A CASSCF/MR-CCI study of the excited states of Fe(CO)$_5$. Chem Phys Lett 1999;302:489–494.

75. Sullivan R, Al-Basheer W, Pagni RM, Compton RN. Linear and non-linear circular dichroism of R-(+)-3-methylcyclopentanone. J Chem Phys 2006;125:144304.

76. Von Grafenstein UB, Bornschlegl A. Circular dichroism laser mass spectrometry, differentiation of 3-methylcyclopentanone enantiomers. ChemPhysChem 2006;7:2085–2087.

77. Snoek LC, van Mourik T, Simons JP. Neurotransmitters in the gas phase: a computational and spectroscopic study of noradrenaline. Mol Phys 2003;101:1239–1248.

78. Butz P, Kroemer RT, Macleod NA, Robertson EG, Simons JP. Conformational preferences of neurotransmitters: norephedrine and the adrenaline analogue, 2-methylamino 1-phenyl ethanol. J Phys Chem A 2001;105:1050–1056.

79. Butz P, Kroemer RT, Macleod NA, Simons JP. Conformational preferences of neurotransmitters: ephedrine and its diastereoisomer, pseudoephedrine. J Phys Chem A 2001;105:544–551.

80. Giardini Guidoni A, Paladini A, Piccirillo S, Rondino F, Satta M, Speranza M. Modelling neurotransmitter functions: a laser spectroscopic study of (1S,2S)-N-methyl pseudoephedrine and its complexes with achiral and chiral molecules. Org Biomol Chem 2006;10:2012–2018.

81. Snoek LC, Robertson EG, Kroemer RT, Simons JP. Conformational landscapes in amino acids: infrared and ultraviolet ion-dip spectroscopy of phenylalanine in the gas phase. Chem Phys Lett 2000;321:49–56.

82. Snoek LC, Kroemer RT, Hockridge M, Simons JP. Conformational landscapes in amino acids: infrared and ultraviolet ion dip spectroscopy of tryptophan. Phys Chem Chem Phys 2001;3:1819–1826.

83. Abo-Riziq AG, Bushnell JE, Crews B, Callahan MP, Grace L, De Vries MS. Discrimination between diastereoisomeric dipeptides by IR-UV double resonance spectroscopy and ab initio calculations. Int J Quantum Chem 2005;105:437–445.

84. Gerhards M, Unterberg C, Gerlach A. Structure of a β-sheet model system in the gas phase: analysis of the C=O stretching vibrations. Phys Chem Chem Phys 2002;4:5563–5565.

85. Unterberg C, Gerlach A, Schrader T, Gerhards A. Structure of the protected dipeptide Ac Val-Phe-OMe in the gas phase: towards a β-sheet model system. J Chem Phys 2003;118:8296.

86. Gerhards M, Unterberg C, Gerlach A, Jansen A. β-sheet model systems in the gas phase: structures and vibrations of Ac–Phe–NHMe and its dimer $(Ac–Phe–NHMe)_2$. Phys Chem Chem Phys 2004;6:2682–2690.

87. Chin W, Compagnon I, Dognon JP, Canuel C, Piuzzi F, Dimicoli I, von Helden G, Meijer G, Mons M. Spectroscopic evidence for gas-phase formation of successive β-turns in a three-residue peptide chain. J Am Chem Soc 2005;127:1388–1389.

88. Chin W, Dognon JP, Canuel C, Piuzzi F, Dimicoli I, Mons M, Compagnon I, von Helden G, Meijer G. Secondary structures of short peptide chains in the gas phase: double resonance spectroscopy of protected dipeptides. J Chem Phys 2005;122:054317.

89. Jockusch RA, Talbot FO, Simons JP. Sugars in the gas phase: the spectroscopy and structure of jet-cooled phenyl β-D-galactopyranoside. Phys Chem Chem Phys 2003;5:1502–1507.

90. Talbot FO, Simons JP. Sugars in the gas phase: the spectroscopy and structure of jet-cooled phenyl β-D-glucopyranoside. Phys Chem Chem Phys 2002;4:3562–3565.

91. Jockusch RT, Kroemer FO, Talbot LC, Snoek P, Çarçabal JP, Simons M, Havenith JM, Bakker I, Compagnon G, Meijer G, von Helden G. Probing the glycosidic linkage: UV and IR ion-dip spectroscopy of a lactoside. J Am Chem Soc 2004;126:5709.

92. Çarçabal P, Huenig I, Gamblin DP, Liu B, Jockusch RA, Kroemer RT, Snoek LC, Fairbanks AJ, Davis BG, Simons JP. Building up key segments of N-glycans in the gas phase: intrinsic structural preferences of the $\alpha(1,3)$ and $\alpha(1,6)$ dimannosides. J Am Chem Soc 2006;128:1976–1981.

93. Brenner V, Piuzzi F, Dimicoli I, Tardivl B, Mons M. Chirality-controlled formation of b-turn secondary structures in short peptide chains: gas phase experiment vs. quantum chemistry. Angew Chem Int Ed 2007;46:2463–2466.

94. Lee KT, Sung J, Lee KJ, Park YD, Kim SK. Conformation-dependent ionization energies of L-phenylalanine. Angew Chem Int Ed Engl 2002;41:4114–4117.

95. Lee KT, Kim HM, Han KY, Sung J, Lee KJ, Kim SK. Spectroscopic observation of conformation-dependent charge distribution in a molecular cation. J Am Chem Soc 2007;129:2588–2592.

96. Zwier TS. The spectroscopy of solvation in hydrogen-bonded aromatic clusters. Annu Rev Phys Chem 1996;47:205–241

97. Robertson EG, Simons JP. Getting into shape: conformational and supramolecular landscapes in small biomolecules and their hydrated clusters. Phys Chem Chem Phys 2001;3:1–18.

98. Çarçabal P, Jockusch RA, Huenig I, Snoek LC, Kroemer RT, Compagnon I, Oomens J, Simons JP. Hydrogen bonding and co-operativity in isolated and hydrated sugars: mannose, galactose, glucose and lactose. J Am Chem Soc 2005;127:11414–11425.

99. Elliott AJ, Hudlicky M, Pavlath AE. Chemistry of organic fluorine compounds. II. A critical review (ACS Monograph 187). Washington, DC: American Chemical Society; 1995. p 1119–1125.

100. Ojima I, McCarthy JR, Welch JT, Editors, Biomedical Frontiers of Fluorine Chemistry, ACS Symposium Series 639, American Chemical Society, Washington, D.C. 1996 (Chapter I) p. 2.

101. Filippi A, Giardini A, Marcantoni E, Paladini A, Piccirillo S, Renzi G, Rondino F, Roselli G, Satta M, Speranza M. Dissymmetry effects on the laser spectroscopy of supersonically expanded rare gas/chiral arene heteroclusters. Phys Chem Chem Phys 2007;14:1676–1679.

102. Giardini A, Rondino F, Cattenacci G, Paladini A, Piccirillo S, Satta M, Speranza M. Van der Waals interactions in a monosolvated chiral fluorinated molecule, R2PI vibroelectronic spectra of (R)-1-phenyl-2,2,2-trifluoroethanol clustered with water. Chem Phys Lett 2007;435:230–235.

103. Giardini A, Piccirillo S, Scuderi D, Satta M, Di Palma TM, Speranza M. Chirality and intermolecular forces: studies using R2PI experiments in supersonic beams. Phys Chem Chem Phys 2000;2:4139–4142.

104. Garret AW, Zwier TS. Multiphoton ionization studies of clusters of immiscible liquids. II. $C_6H_6$-$(H_2O)_n$, $n = 3$–$8$ and $(C_6H_6)_2$-$(H_2O)_{1,2}$. J Chem Phys 1992;96:3402–3410.

105. Veneziani M. Undergraduate Thesis. Università degli Studi di Roma La Sapienza, 1995.

106. Chervenkov S, Wang PQ, Braun JE, Georgiev S, Neusser HJ, Nandi CK. High-resolution ultraviolet spectroscopy of p-fluorostyrene-water: evidence for a s-type hydrogen-bonded dimer. J Chem Phys 2005;122:244312.

107. Bieske EJ, Rainbird MW, Atkinson IM, Knight AEW. Stretch–bend coupling between van der Waals modes in the $S_1$ state of substituted benzene–$Ar_1$ complexes. J Chem Phys 1989;91:752–761.

108. Lu Y, Hu YH, Yang SH. Resonant two-photon ionization spectra of o, p, m-xylene...$Ar_n$ ($n = 1, 2$). Z Phys D 1997;40:40–43.

109. Araki M, Sato S, Kimura K. Two-color zero kinetic energy photoelectron spectra of benzonitrile and its van der Waals complexes with argon. Adiabatic ionization potentials and cation vibrational frequencies. J Phys Chem 1996;100:10542–10546.

110. Takahashi M, Ozeki H, Kimura K. Vibrational spectra of aniline-$Ar_n$ van der Waals cations ($n = 1$ and $2$) observed by two-color "Threshold Photoelectron" [zero kinetic energy (ZEKE)-photoelectron] spectroscopy. J Chem Phys 1992;96:6399–6406.

111. Shinohara H, Sato S, Kimura K. Zero kinetic energy (ZEKE) photoelectron study of fluorobenzene-argon van-der-waals Complexes. J Phys Chem A 1997;101:6736–6740.

112. Douin S, Parneix P, Bréchignac P, Amar FG. Structure, dynamics and spectroscopy of aniline-(argon)n clusters. I. Experimental spectra and interpretation for $n = 1$ to 6. J Phys Chem A 1997;101:122–138.

113. Coreno M, Piccirillo S, Giardini Guidoni A, Mele A, Palleschi A, Brechignac Ph, Parneix P. R2PI detection and spectroscopy of van der Waals complexes of 4-fluorostyrene with rare gases. Chem Phys Lett 1995;236:580–586.

114. Piccirillo S, Consalvo D, Coreno M, Giardini-Guidoni A, Douin S, Parneix P, Bréchignac Ph. Isomeric structures, van der Waals frequencies and spectral shifts of cold 4-fluorstyrene-(argon)[n] clusters ($n = 1$ to 4). Chem Phys 1994;187:97–106.

115. Latini A, Satta M, Giardini Guidoni A, Piccirillo S, Speranza M. Short-range interactions in supersonically formed molecular complexes, structural effects and chiral discrimination. Chem Eur J 2000;6:1042–1049.

116. Filippi A, Giardini A, Piccirillo S, Speranza M. Gas-phase enantioselectivity. Int J Mass Spectrom 2000;198:137–163.

117. Speranza M, Satta M, Piccirillo S, Rondino F, Paladini A, Giardini A, Filippi A, Catone D. Chiral recognition by mass-resolved laser spectroscopy. Mass Spectrom Rev 2005;24:588–610.

118. Giardini A, Cattenacci G, Paladini A, Piccirillo S, Satta M, Rondino F, Speranza M. Monosolvation of R-1-phenyl-2,2,2-trifluoroethanol with amines: configurational effects on the excitation, ionisation and fragmentation of diastereomeric complexes. J Phys Chem A 2007;111:12559–12562.

119. Giardini A, Paladini A, Catone D, Piccirillo S, Rondino F, Satta M, Filippi A, Speranza M, Turchini S, Zema N. Photo-ionization spectroscopy and mass spectrometry of some molecular and supramolecular asymmetric systems in the isolated state. Chirality 2006;18:562–568.

120. Piccirillo S, Rondino F, Catone D, Giardini Guidoni A, Paladini A, Tacconi M, Satta M, Speranza M. Excitation, ionization, and fragmentation of chiral molecules in asymmetric microenvironments: a mass-resolved R2PI spectroscopic study. J Phys Chem A 2005;109:1828–1835.

121. Giardini Guidoni A, Paladini A, Rondino F, Piccirillo S, Satta M, Speranza M. Chiral clusters in a supersonic beam: R2PI-TOF spectroscopy of diastereomeric carboxylic esters/(R)-(+)-1-phenyl-1-propanol complexes. Org Biomol Chem 2005;3:3984–3989.

122. Giardini Guidoni A, Piccirillo S, Scuderi D, Satta M, Di Palma TM, Speranza M, Filippo A, Paladini A. R2PI study of intermolecular hydrogen bond in solvent-free chiral complexes. Chirality 2001;13:727–730.

123. Latini A, Toja D, Giardini-Guidoni A, Palleschi A, Piccirillo S, Speranza M. Spectroscopic enantiodifferentiation of chiral molecules in the gas phase. Chirality 1999;11:376–380.

124. Lavrich RJ, Torok CR, Tubergen MJ. A microwave spectroscopic investigation of the networked structure of 3-hydroxytetrahydro-furan-$H_2O$. J Phys Chem A 2001;105:8317–8322.

125. Giuliano BM, Ottavini P, Favero LB, Caminati W, Grabow JU, Giardini A, Satta M. Conformational preferences of chiral molecules: free jet rotational spectrum of 1-phenyl-1-propanol. Phys Chem Chem Phys 2007;9:4460–4464.

126. Giardini-Guidoni A, Piccirillo S, Palleschi A, Toja D. Resonance enhanced multiphoton ionization processes to study spectroscopy and reactivity of van der Waals cluster of aromatic molecules. Proc Indian Acad Sci 1998;110:153–162.

127. Scuderi D, Paladini A, Piccirillo S, Satta M, Catone D, Giardini A, Filippi A, Speranza M. Chiral discrimination of 2,3-butanediols by laser spectroscopy. Chem Commun 2002;20:2438–2439.

128. Piccirillo S, Satta M, Catone D, Scuderi D, Paladini A, Rondino F, Speranza M, Giardini Guidoni A. Mass resolved laser spectroscopy of micro-solvated R-(+)-1-phenyl-1-propanol: a chiral molecule of biological interest. Phys Chem Chem Phys 2004;6:2858–2862.

129. Van Scott EJ, Yu RJ. α hydroxy acids: procedures for use in clinical practice. Can J Dermatol 1989;43:222–228.

130. Kleerebezem M, Hugenholtz J. Metabolic pathway engineering in lactic acid bacteria. Curr Opin Biotechnol 2003;14:232–237.

131. Dian BC, Clarkson JR, Zwier TS. Direct measurement of energy thresholds to conformational isomerization in tryptamine. Science 2004;303:1169–1173.

132. Zhu L, Johnson P. Mass analyzed threshold ionization spectroscopy. J Chem Phys 1991;94:5769–5771.

133. Zewail AH. Femtochemistry: ultrafast dynamics of the chemical bond. Singapore: World Scientific; 1994. (20th Century Chemistry Series).

134. Dermota TE, Zhong Q, Castleman AW Jr. Ultrafast dynamics in cluster systems. Chem Rev 2004;104:1861–1886.

135. Hertel IV, Radloff W. Ultrafast dynamics in isolated molecules and molecular clusters. Rep Prog Phys 2006;69:1897–2003.